DOPING EFFECT ON THE ANODE MATERIAL CAPABILITY OF 2D BN NANOSHEETS

A Thesis Submitted to
the Graduate School of Engineering and Sciences of
İzmir Institute of Technology
in Partial Fulfillment of the Requirements for the Degree of

MASTER OF SCIENCE

in Chemistry

by
Mustafa Coşkun ÖZDEMİR

March 2024
İZMİR

We approve the thesis of **Mustafa Coşkun ÖZDEMİR**

Examining Committee Members:

_____

Prof. Dr. Nuran Elmacı IRMAK

Department of Chemistry, Izmir Institute of Technology

_____

Prof. Dr. Talat YALÇIN

Department of Chemistry, Izmir Institute of Technology

_____

Prof. Dr. Elif IŞGIN

Department of Chemistry, Dokuz Eylul University

1 March 2024

_____

Prof. Dr. Nuran Elmacı IRMAK

Supervisor, Department of Chemistry

Izmir Institute of Technology

_____

Prof. Dr. Gülşah Şanlı MOHAMED

Head of the Department of Chemistry

_____

Prof. Dr. Mehtap EANES

Dean of the Graduate School of Engineering and Sciences

ACKNOWLEDGEMENTS

I owe a debt of gratitude to everyone who has stood by me and offered their support throughout this academic journey. First and foremost, I would like to sincerely thank my supervisor, Prof. Dr. Nuran Elmacı Irmak, for all her unwavering support, the opportunities she provided, her understanding, and for enabling me to discover and advance in the field of computational chemistry. Without her belief in me and her guidance, this thesis would not have been possible.

I just wanted to express my sincere gratitude to every member of the Elmacı research group. Throughout my master's studies, I had the pleasure of spending some truly enjoyable times with all of you, and I am so grateful for the way you made it possible for me to work in the lab without ever getting bored. I would like to extend special thanks you to Erman Kıbrıs, Nehir Nalıncı Barbak, Seval İkizoğlu, and Zelal Agin. Your contributions have meant more to me than you could possibly know.

I would also like to express my gratitude to the committee members who evaluated my work, Prof. Dr. Talat Yalçın and Prof. Dr. Elif Işgın, for their valuable contributions and insights.

I convey my love to my family for the endless trust, love, and belief they have shown me on this journey. Lastly, I am grateful to my friends Batuhan Mergüz and Berkay Yılmaz, who have put up with me on this journey, motivated me with their understanding, and have always been by my side.

ABSTRACT

Doping Effect on the Anode Material Capability of 2D BN Nanosheets

In this thesis, the potential of BNN surfaces doped with Al, Cl, Co, Fe, Ga, O, P, and S atoms as anode materials in K, Li, Mg, and Na ion batteries was investigated. Semi-empirical tight-binding combined with meta-dynamics methods and density functional theory were utilized to discover these properties. The effects of doping atoms on the electronic structure and geometry of BNN surfaces were also studied. Changes in the electronic structure and conductivity were reported by examining the HOMO-LUMO orbitals and the energy differences between these orbitals.

Using previously reported experimental data and examining similar studies from the literature, the atoms to be doped were chosen. While vacancies at the sites of boron atoms in single-layer boron-nitride nanosheets were observed, vacancies formed by nitrogen atoms were not observed, indicating that boron vacancies are much more likely for the doping position. So that doping was performed on the boron atom. The level of quantum calculations used in this work was validated using experimental data. B3LYP/def2-SVP/D4/gCP level of theory is used for all calculations for BNN-nanosheets studied in this thesis. The bond lengths and the HOMO-LUMO energy difference were found to be nearly the same as the experimental data.

The conductivity of the BNN surface was increased with the doping process. However, significant improvements are followed by doping of cobalt, iron, and sulfur atoms with 35%, 34%, and 26% alteration, respectively. For a suitable battery manufacture, the potential anode material should offer structures with high theoretical specific capacity, low anode electrode voltage, and minimal volume change between charged/discharged states. It was observed that none of the doped-BNN surfaces involved in this study were suitable for the use of anode material in magnesium ion batteries. On the other hand, they can be used as a negative electrode for potassium, lithium, and sodium batteries. Their capacity in lithium is better than Na and K batteries. Our results suggest that most of the doped BNN surface with ions studied in this thesis could be used as anode materials. However, none of them owns a better battery capacity than classic lithium batteries.

ÖZET

2 Boyutlu BN Nanotabakaların Anot Malzemesi Olma Kapasitesi Üzerine Doping Etkisi

Bu tezde, Al, Cl, Co, Fe, Ga, O, P, S atomları ile katkılandırılmış (doped) edilmiş BNN yüzeylerinin K, Li, Mg, Na iyon bataryalarında anot materyal olarak kullanılma potansiyeli incelenmiştir. Bu özellikleri keşfetmek için yarı deneysel sıkı bağlama yöntemleri ile meta-dinamik yöntemler ve yoğunluk fonksiyonel teorisi kullanılmıştır. Katkılanan atomlarının BNN yüzeylerinin elektronik yapısı ve geometrisi üzerindeki etkileri de incelenmiştir. Elektronik yapıdaki ve iletkenlikteki değişimleri, HOMO-LUMO orbitalleri ve bu orbitaller arasındaki enerji farklılıkları inceleyerek raporlanmıştır.

Daha önce raporlanmış deneysel veriler kullanılarak ve literatürde benzer çalışmalar incelenerek katkılanacak atomlar seçilmiştir. Tek katmanlı bor-nitrit nano-tabakalarda boron atomlarının olduğu noktalarda boşluklar gözlemlenebilirken, nitrojen atomlarının oluşturduğu boşluklar gözlemlenmemiştir. Bu durum, doping pozisyonu için boron boşluklarının çok daha olası olduğunu göstermektedir. Bu nedenle doping, boron atomu üzerinde gerçekleştirilmiştir. Bu çalışmada kullanılan kuantum hesaplamaların seviyesi deneysel veriler kullanılarak doğrulanmıştır. BNN-nano-tabakalar için tüm hesaplamalarda B3LYP/def2-SVP/D4/gCP teori seviyesi kullanılmıştır. Bağ uzunlukları ve HOMO-LUMO enerji farkı, deneysel verilerle neredeyse aynı bulunmuştur.

BNN yüzeyinin iletkenliği doping işlemi ile artırılmıştır. Ancak, kobalt, demir ve sülfür atomlarıyla katkılama sırasıyla %35, %34 ve %26'lık önemli iyileştirmeler sağlamıştır. Uygun bir pil üretimi için, anot materyalin yüksek teorik spesifik kapasiteye, düşük anot elektrot voltajına ve yüklü/yüksüz durumlar arasında minimal hacim değişimine sahip olmalıdır. Hiçbir katkılı-BNN yüzeyinin magnezyum iyon pillerinde kullanılmak için uygun olmadığı gözlemlenmiştir. Öte yandan, potasyum pilleri, lityum ve sodyum pillerine benzer performans göstermiş olmasına rağmen lityum piller en iyi performansı sergilemiştir. Sonuçlarımız, bu tezde incelenen iyonlarla katkılanmış çoğu BNN yüzeyinin anot materyali olarak kullanılabileceğini göstermektedir. Ancak, hiçbiri klasik lityum pillerinden daha iyi bir pil kapasitesine sahip değildir.

TABLE OF CONTENTS

LIST OF FIGURES vii

LIST OF TABLES ix

CHAPTER 1 INTRODUCTION 1

1.1. Batteries 1
1.2. Li-ion Batteries 2
1.3. Na-ion Batteries 3
1.4. Mg-ion Batteries 4
1.5. K-ion Batteries 6
1.6. BN Nanosheets (BNN) 7

CHAPTER 2 COMPUTATIONAL METHODS 9

2.1. Density Functional Theory 9
2.2. Computational Aspects 10
2.2.1. Conformer-Rotamer Ensemble Sampling Tool (CREST) 10
2.2.2. ORCA Quantum Chemistry Package 12
2.3. Analysis Methods 12
2.4. Aim of the Study 13

CHAPTER 3 RESULT AND DISCUSSION 15

3.1. Structures of Doped-BNNs 15
3.2. Electronic Structure of Doped-BNNs 25
3.3. Anode Material Capability 34

CHAPTER 4 CONCLUSION 52

REFERENCES 54

LIST OF FIGURES

Figure **Page**

Figure 1.1. NAS battery cell principle of operation (Source: Oshima, Kajita, and Okuno 2004) 3
Figure 1.2. A boron monovacancy. (a) The phase image of reconstructed exit wave of a region containing a boron monovacancy. (b) A line profile confirms the missing atom is boron. (c) Simulated phase image and (d) line profile involving the boron monovacancy. Scale bar = 0.2 nm. (Source: Jin et al. 2009) 7
Figure 1.3. Crystal structures of (a) graphite and (b) h-BN. (Source: Tsuji et al. 2019).. 8
Figure 2.1. Schematic Schematic 1-D PES that is "filled" by several bias potentials over time, which allows larger barrier heights to be overcome. (Source: Pracht, Bohle, and Grimme 2020) 11
Figure 3.1. Optimized Boron-nitride nanosheet, dopant position (D) and nearest nitrogen atoms to the dopant (N1, N2, N3) 15
Figure 3.2. Top view and side view of optimized Al-doped BNN structure 17
Figure 3.3. Top view and side view of optimized Cl-doped BNN structure 18
Figure 3.4. Top view and side view of optimized Co-doped BNN structure 19
Figure 3.5. Top view and side view of optimized Fe-doped BNN structure 20
Figure 3.6. Top view and side view of optimized Ga-doped BNN structure 21
Figure 3.7. Top view and side view of optimized O-doped BNN structure 22
Figure 3.8. Top view and side view of optimized P-doped BNN structure 23
Figure 3.9. Top view and side view of optimized S-doped BNN structure 24
Figure 3.10. HOMO, LUMO orbitals of pristine BNN 26
Figure 3.11. HOMO, LUMO orbitals of Al-doped BNN 27
Figure 3.12. HOMO, LUMO orbitals of Cl-doped BNN 28
Figure 3.13. HOMO, LUMO orbitals of Co-doped BNN 29
Figure 3.14. HOMO, LUMO orbitals of Fe-doped-BNN 30
Figure 3.15. HOMO, LUMO orbitals of Ga-doped BNN 31

Figure **Page**

Figure 3.16. HOMO, LUMO orbitals of O-doped BNN 32
Figure 3.17. HOMO, LUMO orbitals of P-doped BNN 33
Figure 3.18. HOMO, LUMO orbitals of S-doped BNN 34
Figure 3.19. Optimized structure of ion loaded top and side view of Al-doped BNN ... 36
Figure 3.20. Optimized structure of ion loaded top and side view of Cl-doped BNN ... 38
Figure 3.21. Optimized structure of ion loaded top and side view of Co-doped BNN .. 40
Figure 3.22. Optimized structure of ion loaded top and side view of Fe-doped BNN ... 42
Figure 3.23. Optimized structure of ion loaded top and side view of Ga-doped BNN .. 44
Figure 3.24. Optimized structure of ion loaded top and side view of O-doped BNN 46
Figure 3.25. Optimized structure of ion loaded top and side view of P-doped BNN..... 48
Figure 3.26. Optimized structure of ion loaded top and side view of S-doped BNN..... 51

LIST OF TABLES

Table **Page**

Table 3.1 Distances between the dopant and nearest nitrogen atoms in Å and dihedral angle of N1-N2-N3-D 16

Table 3.2 HOMO-LUMO energies, energy gap of the pristine BNN and doped-BNNs, and percent change in the energy gap with respect to the pristine BNN. 25

Table 3.3. Adsorption energy (E_{ads}), voltage of the corresponding negative electrode material (V_{cell}), theoretical specific capacity (C_c) and theoretical volume change between the charged and discharged states (ΔV) for 100 g of material of Al-doped BNN 37

Table 3.4. Adsorption energy (E_{ads}), voltage of the corresponding negative electrode material (V_{cell}), theoretical specific capacity (C_c) and theoretical volume change between the charged and discharged states (ΔV) for 100 g of material of Cl-doped BNN 38

Table 3.5. Adsorption energy (E_{ads}), voltage of the corresponding negative electrode material (V_{cell}), theoretical specific capacity (C_c) and theoretical volume change between the charged and discharged states (ΔV) for 100 g of material of Co-doped BNN 40

Table 3.6. Adsorption energy (E_{ads}), voltage of the corresponding negative electrode material (V_{cell}), theoretical specific capacity (C_c) and theoretical volume change between the charged and discharged states (ΔV) for 100 g of material of Fe-doped BNN 42

Table 3.7. Adsorption energy (E_{ads}), voltage of the corresponding negative electrode material (V_{cell}), theoretical specific capacity (C_c) and theoretical volume change between the charged and discharged states (ΔV) for 100 g of material of Fe-doped BNN 44

Table 3.8. Adsorption energy (E_{ads}), voltage of the corresponding negative electrode material (V_{cell}), theoretical specific capacity (C_c) and theoretical volume change between the charged and discharged states (ΔV) for 100 g of material of O-doped BNN 46

Table **Page**

Table 3.9. Adsorption energy (E_{ads}), voltage of the corresponding negative electrode material (V_{cell}), theoretical specific capacity (C_c) and theoretical volume change between the charged and discharged states (ΔV) for 100 g of material of P-doped BNN 48

Table 3.10. Ion capacities and their nearest distances (Å) from the doped surfaces. 50

Table 3.11. Adsorption energy (E_{ads}), voltage of the corresponding negative electrode material (V_{cell}), theoretical specific capacity (C_c) and theoretical volume change between the charged and discharged states (ΔV) for 100 g of material of S-doped BNN 51

CHAPTER 1

INTRODUCTION

1.1.Batteries

The history of batteries starts with Alessandro Volta's invention of the Voltaic Pile in 1800, which was the first device to produce a steady electrical current chemically. Progress continued with the development of the lead-acid battery by Gaston Planté in 1859, the first rechargeable battery. Over the years, technology evolved to include nickel-cadmium (NiCd) rechargeable batteries in 1899, followed by significant advancements in the 20th century like alkaline, nickel-metal hydride (NiMH), and lithium-ion batteries. Lithium-ion batteries, emerging in the 1990s, have become pivotal for portable electronics and electric vehicles due to their high energy density and durability. Today, battery technology continues to advance, focusing on higher efficiency and sustainability.

Technological and industrial improvements demand high energy as they proceed. Especially, transformation of transportation from fossil fuel-powered vehicles to electric vehicles requires sustainable rechargeable batteries. Energy density is one of the most important aspects of rechargeable batteries because it provides portability, which paves the way for the development of portable, small-sized electronic devices such as the Internet of Things (IoTs) and cell phones. Another important property is that maximum battery life cycle which contributes to sustainability. Today, efforts on to reduce greenhouse gas emission by academy and industry is getting more important as the climate change affect our lives. Unfortunately, most of the individual renewable energy sources cannot supply energy constantly. Therefore, energy storage technologies are getting more importance as the renewable energy sources become more popular. Yet, production of such technologies should also be environment friendly. Otherwise, reduction on the fossil-fuel usage would not effectively reduce greenhouse gas emission.

1.2.Li-ion Batteries

Today, li-ion batteries (LIBs) are the most widely used rechargeable batteries (M. Li et al. 2018). There are many reasons for it to be so. Lithium, being the third lightest element, possesses the smallest ionic radius among ions with a single charge. It also has the lowest reduction potential, resulting in the highest potential for cell voltage (Nitta et al. 2015). These basic properties make LIBs promising commercial batteries. Although research on LIBs dates back to the 1970s, LIBs were successfully produced commercially in 1991 by a Sony and Asahi Kasei (Goikolea et al. 2020). LIBs have relatively high energy density, low capacity fading per cycle, low volume changes during electrochemical cycling. For example, silicon as an anode material in LIBs has higher theoretical capacity. However, it faces problems, such as large volume changes during charging and discharging, leading to cracking, pulverization, and rapid capacity decay. The most common anode material for the LIBs is graphite, which provide approximately, 372 mAh/g specific capacity (Jingxing Wu et al. 2019; Peled et al. 1996). Safety and reliability concerns are the most important topic about the batteries, especially in electric vehicles. Under certain conditions batteries poses risks. Especially, upon an oxidation or at elevated temperatures, solid electrolyte interphase (SEI) layer can break down and which could cause a thermal runaway potentially leading to a fire or explosion (Chombo and Laoonual 2020).

There are several experimental and theoretical studies to offer a promising alternative to traditional anode materials to achieve higher energy densities, longer life cycles and faster charging rates. Shao and coworkers developed a composite made of silicon oxycarbide (SiOC), derived from a polymer, integrated with a graphene aerogel, which achieved a stable reversible charge capacity of 751 mAh/g at low charge rates (Shao et al. 2020). Alternatively, another study is explored the theoretical investigation of anode material capability of Si-doped γ-Graphyne against lithium ion. Density functional theory (DFT) and Ab Initio Molecular Dynamics (AIMD) simulations are revealed that, favorable binding energies, high specific capacity, 1005.05 mAh/g, small diffusion barrier and desirable average voltage (Duhan and Dhilip Kumar 2024). Open circuit voltage (OCV) should not be very high or low to reduce safety risks such as formation of dendrites which may cause an internal short circuit (Y. Huang et al. 2019; L. Li et al. 2021).

1.3.Na-ion Batteries

Sodium is one of the most abundant element on earth and in the seas, and the second lightest alkali metal after lithium. However, it's larger ionic radius compared to lithium may make it more difficult to maintain structural stability between cycles (Saritha and Sujithra 2023). Sodium is much more abundant compared to lithium, making it a desirable element for large-scale production facilities. The rapid increase in the number of devices required by portable battery technology and industrial needs has led to the search not only for high-energy-capacity batteries but also for cheap and durable alternatives (Kubota and Komaba 2015). Historically, the first reversible sodium anode cell (Na-TiS_2) operating at room temperature was produced in 1980. However, the dramatic drop in voltage after the first few cycles emphasized that this system was not practical because it showed that the anode material's structure did not remain stable between cycles (Newman and Klemann 1980).

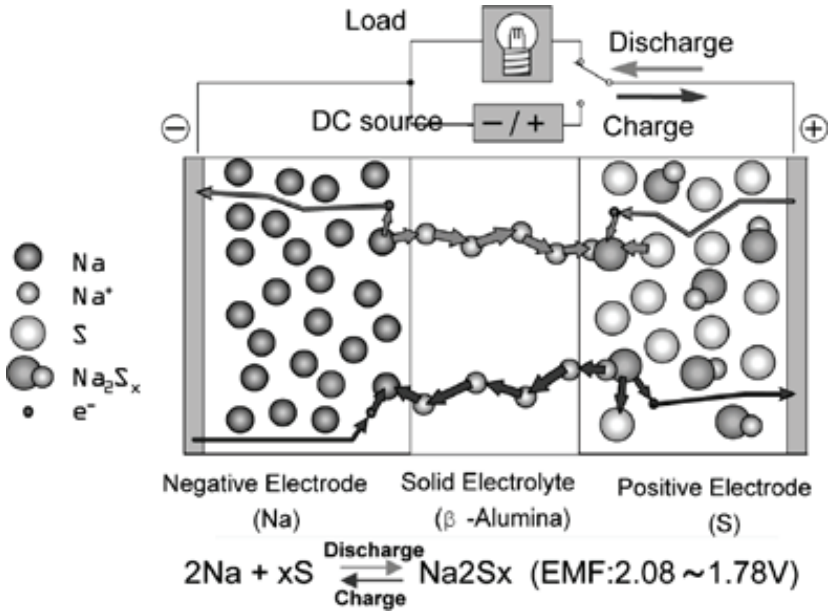

Figure 1.1. NAS battery cell principle of operation (Source: Oshima, Kajita, and Okuno 2004)

Due to the overwhelming success of lithium batteries, research into sodium-based batteries did not gain popularity for a long time (Gu et al. 2024). The limited resources of lithium and the high costs associated with it made the integration into large-scale storage

systems challenging, delaying the search for new resources. However, the discovery of sodium batteries capable of operating at high temperatures, such as Na_2S_x (Hueso, Armand, and Rojo 2013) began to draw more interest towards sodium batteries (see Figure 1.1), especially with the issues experienced with lithium, and continued with sodium-oxygen batteries (W. Liu et al. 2013). For instance, sodium-sulfur (NAS) batteries operating at 300 degrees with β-alumina solid electrolyte (Oshima, Kajita, and Okuno 2004), or Na/O2 batteries developed with carbon nanotubes and graphene nanosheets (Jian et al. 2014).

In a study like this thesis, a boron-nitride nanosheet (BNN) was introduced, and a DFT study was conducted on it as an anode material for Na-ion batteries. Phosphorus-doped BNN emerged as a promising material for Na-ion batteries, producing a cell voltage of approximately 2.13 V (Hosseinian et al. 2017). Not only doping but also encapsulation can boost the electronic structure of anode materials by altering it. While the $B_{12}N_{12}$ nanocluster yields a low voltage in interaction with Na-ion, after halide encapsulation, it possesses a high voltage (Nejati et al. 2017). In another DFT study, it is shown that doping a phagraphene nanosheet with boron and nitrogen could make it a suitable material for Na-ion batteries. The lone pairs on the nitrogen atoms contribute to an increase in the cell voltage (Saadh et al. 2024). Since 2010, research on Na-ion batteries has gained significant momentum, and not only theoretical but also experimental studies have begun to emerge (Kubota and Komaba 2015). One of the recent developments is the high performance of the low-cost chiolite mineral containing sodium, titanium, and iron in Na-ion batteries. This battery operates at low voltages while having high Coulombic efficiency and provides reversible conversion-deconversion reactions during charge-discharge cycles (Kang et al. 2023). Despite findings on Na-ion batteries in 1980′s, today, however, the Swedish-based company Northvolt has introduced commercial sodium-ion batteries, and the China-based Contemporary Amperex Technology Co. (CATL) is planning to use sodium-ion batteries in electric vehicles and move to the industrial production stage of these batteries (Anthony King 2023).

1.4.Mg-ion Batteries

Like sodium, magnesium is much more abundant on Earth than lithium, making it more accessible. Although magnesium cations have a +2 charge, which is expected to

give Mg-ion batteries (MIBs) a higher capacity, this is not always the case, and it can sometimes reduce ion mobility (Massé, Uchaker, and Cao 2015). One of the greatest challenges with Mg-ion batteries, particularly, is the corrosive effects of electrolytes containing chloride on battery components. The formation of a thick solid electrolyte interphase (SEI) on the anode (with traditional electrolytes) can lead to the formation of an irreversible passivating layer, which hinders the movement of Mg2+ ions. When the ions become trapped on the anode, this results in a decrease in Coulombic efficiency (Lu et al. 1999). Overcoming this problem relies on relatively recent studies, dating back approximately a decade (Y. Guo et al. 2012; Tutusaus et al. 2015; Nelson et al. 2014). Despite this and similar solutions, MIBs still harbor many practical issues. One of these is the low reversible capacity due to the inability of magnesium, being a divalent structure, to diffuse properly towards the cathode material (Shterenberg et al. 2014; Q. Guo et al. 2021).

Candidates for anode materials that can work effectively with Mg-ion batteries have been demonstrated in many DFT studies. In one such study, it was shown that a silicon carbide (SiC) monolayer has a low voltage and achieves a theoretical capacity of 683.99 mAh/g, with the system's conductivity also demonstrated (Kadhim et al. 2023). Tin Diselenide ($SnSe_2$) is another potential structure for a Mg-ion battery anode material. Using density functional theory, the scenarios of intercalation, conversion reaction, and alloying reaction between Mg^{2+} ions and $SnSe_2$ have been separately investigated. The highest voltage (1.1 V) is observed in the intercalation process, which demonstrates that this material could be a competitive and promising anode (Chakrabarti, Singh, and Thakur 2023). In one of the recent studies, 2D metal borides, similar to this thesis work, have been examined as anode materials against metal ions (Li, Na, K, Mg). Low energy barriers, which do not hinder the migration of ions, have been demonstrated, with the highest theoretical capacity found for a well-stabilized CrB monolayer (Y. Wang et al. 2024). In another DFT study, the properties of boron doped, and nitrogen doped graphene for Mg-ion batteries were examined. The structure doped with boron yielded much better results compared to the one doped with nitrogen. The study showed that there was no bond formation between the increasing number of ions and Mg ions, and it demonstrated that this material is promising as an anode in Mg-ion batteries (Riyaz et al. 2022). In addition to cage and monolayer structures, nanotube structures are also used in these types of studies. For example, it has been demonstrated through DFT calculations that AlN

nanotubes can be used as a negative electrode material in Mg-ion batteries (Mei et al. 2021).

1.5.K-ion Batteries

Currently, the relative expense and irregular distribution of lithium on Earth prevent lithium-ion batteries from being used as desired in sustainable, large-scale energy storage systems. This situation prompts a search for low-cost, abundantly available elements as alternatives to lithium. Alongside sodium and magnesium, potassium is another important metal resource in this quest. While lithium has the lowest reduction potential at -3.04 V, potassium comes second with a reduction potential of -2.92 V. This characteristic provides a high potential for cell voltage and high energy density. In some solvents, potassium cation's smaller Stokes radius and lower desolvation energy facilitate its diffusion and increase conductivity, making it a viable factor for battery operation. However, the large radius of potassium can hinder intercalation/deintercalation processes, potentially resulting in poor cycling stability (S. Liu et al. 2021). This situation also causes significant volume changes in the battery during ion migration processes, posing safety risks. For reasons like these, KIBs are mostly in prototype stages rather than being practically usable, as seen in most studies (Thakur et al. 2022). However, considering the development processes of other batteries, it is possible to see their practical applications in the near future.

Similar to other batteries, experimental and theoretical studies are observed in potassium-ion batteries. It is known that doping graphene structures with nitrogen, changes the atomic charge distribution and the hybridization between nitrogen's lone pair and carbon's p electron alters the electronic structure and increases activity (H. Wang, Maiyalagan, and Wang 2012). In a study conducted in 2016, it was found that nitrogen-doped graphene layers have a 26% better theoretical capacity for K-ion batteries compared to pristine graphene (Share et al. 2016). In another study, it has been shown through first-principal studies that two-dimensional carbon-nitride monolayer structures are promising anode materials for sodium-potassium ion batteries. The most stable adsorption sites were identified, and a high storage capacity of 1076 mAh/g was found (Bhauriyal, Mahata, and Pathak 2018). In another study, a carbon nanotube (CNT)-containing dipotassium terephthalate composite electrode was confirmed experimentally

by XRD and FTIR spectroscopy, and theoretical studies also demonstrated the stability of the intercalation of potassium atoms (Ghosh et al. 2020). In a similar study to this thesis, di-boron di-nitride monolayer (o-B_2N_2) shows promising properties as an anode for potassium ion batteries (Rajhi et al. 2023).

1.6.BN Nanosheets (BNN)

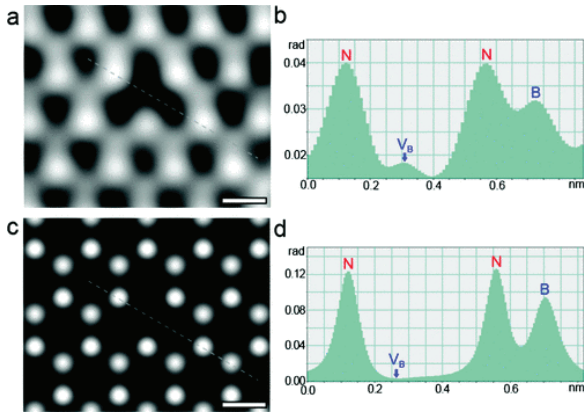

Figure 1.2. A boron monovacancy. (a) The phase image of reconstructed exit wave of a region containing a boron monovacancy. (b) A line profile confirms the missing atom is boron. (c) Simulated phase image and (d) line profile involving the boron monovacancy. Scale bar = 0.2 nm. (Source: Jin et al. 2009)

Boron-nitride nanosheets (BNN) crystals were first synthesized in 2004. This material primarily exhibits properties suitable for use in ultraviolet laser devices. Which poses materials with a wide electronic band gap. Similar to BNN, gallium nitride (GaN) and aluminum nitride (AlN) are also suitable for use in such devices. The main requirement in these devices is a high band gap energy. BNN, GaN, and AlN have band gaps of approximately 5.77 eV, 3.4 eV, and 6.42 eV, respectively (Watanabe, Taniguchi, and Kanda 2004). However, for a material to be an ideal anode material, it first needs to be a good conductor. In this study, BNN structures were doped with certain materials to investigate changes in the electronic structure to explore if they reduce the band gap energy and so increase conductivity of BNN 2D material. There are two possibilities for doping BNN structures, meaning doping should be applied via either boron or nitrogen atoms. A study in 2009 sheds light on this thesis. For the first time then, freestanding boron nitride single layer was observed. In that study, defects on the hexagonal boron

nitride monolayer were revealed using high-resolution transmission electron microscopy (HRTEM) and the exit-wave reconstruction method, and monovacancies were determined (Jin et al. 2009). Many boron monovacancies were identified, but no nitrogen monovacancies were found (see Figure 1.2). Therefore, doping boron atoms in the structure is much more likely, and this study was conducted accordingly.

Numerous studies have examined the suitability of using other two-dimensional materials besides the BNN structure. It was reported that the doping methods altered their electronic structure to improve their anode material properties. For example, research has been conducted on silicon-doped titanium carbide (Ti_2C) (Das et al. 2022), cobalt-doped α-Fe_2O_3/Graphene (C. Li et al. 2023), and silicon-doped graphene for lithium-ion batteries (H. Liu et al. 2022). Nitrogen-doped graphene has been studied for zinc-ion batteries (Sun et al. 2024), while silicon and boron doped phosphorus carbides (PC_3) have been studied for sodium-ion batteries (L. Liu et al. 2023).

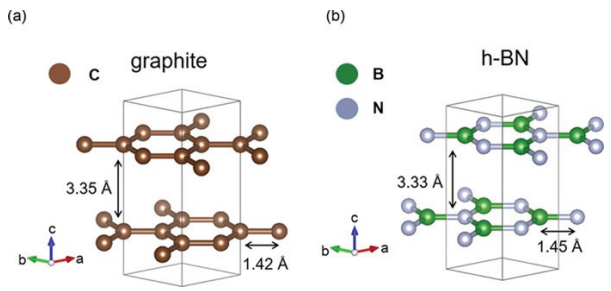

Figure 1.3. Crystal structures of (a) graphite and (b) h-BN. (Source: Tsuji et al. 2019)

Given that graphite is the most extensively utilized anode material in Li-ion batteries, it is worthwhile to draw a comparison with hexagonal boron-nitride (h-BN) nanosheets. Both materials exhibit low thermal expansion, and their interlayer distances are nearly identical, being 3.35 Å for graphite and 3.33 Å for h-BN, respectively (see Figure 1.3). Similarly, the carbon-carbon atomic distance (1.42 Å) and the boron-nitride atomic distance (1.44 Å) are closely matched. Both materials are chemically inert. The most notable distinction between them lies in their conductivity: graphite serves as a good electrical conductor, whereas h-BN is an electrical insulator. However, the conductivity of h-BN can be enhanced through appropriate doping. The most significant contribution to the interlayer bond energy comes from the nonpolar C-C interlayer bonds in graphite and the highly polar B-N bonds in h-BN (Hod 2012).

CHAPTER 2

COMPUTATIONAL METHODS

2.1.Density Functional Theory

Density functional theory (DFT) is a modern tool for investigating electronic properties of materials within an acceptable margin of error, such as bond energies, barrier heights, non-covalent interactions, excitation energies, charge transfer and spectroscopic properties etc.

The root of the quantum chemistry is connected with solving attempts of the Schrödinger equation. The most fundamental wavefunction-based approach is Hartree-Fock (HF) method (Szabo and Ostlund 2012) in which overall many-electron wavefunction of a system is approximated by a single Slater determinant. The main drawback of the HF approximation is that movement of the electrons do not affect each other. In other words, it neglects electron correlation. To recover the electron correlation and reach to the exact wavefunction, more precise approximations are available. They generally called post-HF approximations. For example, Møller-Plesset perturbation theory, configuration interaction, coupled cluster, multi-reference methods etc. Each of these methods has its strengths and weaknesses, they provide the missing part of the correlation energy of the HF approximation, and the choice of method depends on the particular study. However, post-HF methods are more expensive than DFT. At this point, DFT offers to compensate inaccuracy in HF and lower computational cost than post-HF methods.

The root of the density functional theory is connected with two Hohenberg-Kohn theorems (Hohenberg and Kohn 1964). The first theorem states that there is an unique electron density rather than wave-function, and it consists of ground state properties of many-electron system. The second theorem states that total energy of the system is a functional of the electron density and reaches its minimum value for the correct ground state density. Thanks to this approach, we have the opportunity to skip the solution of the many-body Schrödinger equation. Although, Hohenberg-Kohn theorems determined the foundation of the DFT, the practical implementation of DFT is achieved by Kohn-Sham

equations (Kohn and Sham 1965). The Kohn-Sham system simplifies the complexity of the many-electron problem by constructing of a non-interacting system that provides a simplified yet accurate enough description of the electron density as the original problem. The Kohn-Sham system can be described by the following equation:

$$\left[-\frac{\hbar^2}{2m}\nabla^2 + V_{eff}(r)\right]\psi_i(r) = \varepsilon_i\psi_i(r) \tag{2.1}$$

where $\psi_i(r)$ are the Kohn-Sham orbitals, ε_i are the orbital energies, $V_{eff}(r)$ is the effective potential, $\hbar$ is the reduced Planck constant, m is the electron mass and ∇^2 is the Laplacian operator, representing the kinetic energy of the electrons. Therefore, the density for an N-particle system is

$$\rho(r) = \sum_i^N |\psi_i(r)|^2 \tag{2.2}$$

In a noninteracting system, a Slater determinant of orbitals could represent the wavefunction. However, exchange-correlation functional is the only unknown in the Kohn-Sham approach except for the free electron gas, and the main problem of the DFT emerges at this point. To solve the issue, there are many exchange-correlation approximations such as, local-density approximation, generalized gradient approximation etc. which influence the accuracy of the Kohn-Sham method directly (Orio, Pantazis, and Neese 2009).

2.2.Computational Aspects

2.2.1.Conformer-Rotamer Ensemble Sampling Tool (CREST)

The two-dimensional square-shaped hexagonal boron-nitride structure ($B_{33}N_{33}H_{22}$) structure was first created using Python code. All distances between boron and nitrogen atoms were set to the reference value of 1.45 Å, and the outer atoms were saturated with hydrogen atoms to minimize the boundary effect (Amorim et al. 2013).

Since the pristine structure and doped structures have 88 atoms, the degrees of freedom are 258, which is relatively high and makes geometry optimization more

challenging as it increases. Therefore, these structures created with Python code were not directly optimized with DFT. Initially, a pre-optimization was performed using the Conformer-Rotamer Ensemble Sampling Tool (CREST) program (Pracht, Bohle, and Grimme 2020). The CREST program utilizes semiempirical tight-binding methods with meta-dynamics driven search algorithm. This algorithm runs with the GFN2-xTB method, and the lowest energy conformer is selected for DFT optimization. The GFN2-xTB method, developed especially for organic, organometallic, and biochemical systems, uses element-specific parameters, unlike semiempirical methods such as PM6, which use element pair-specific parametrization. On account of the used parametrization and techniques, with this method, it is possible to perform calculations like geometry optimization and vibrational frequencies for a few hundred atoms up to the 86th element (Radon) in the periodic table at the GFN2-xTB level (Bannwarth, Ehlert, and Grimme 2019).

The CREST program applies meta-dynamics simulation to find different conformers, rather than simply altering angles or dihedral angles for generation. The logic of this algorithm is essentially to create a potential energy surface (PES) while finding different conformers with the help of root-mean-square deviation (RMSD) of atomic Cartesian coordinates. As different conformers are found and different minima on the PES are identified, the guiding force applied to the atoms enables the molecule's geometry to overcome barriers and scan the PES. Therefore, this method makes it possible to find "true" quantum chemical energy minima for some structures (see Figure 2.1).

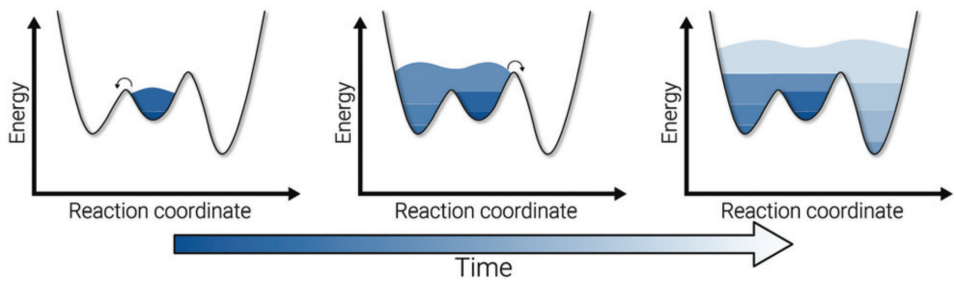

Figure 2.1. Schematic Schematic 1-D PES that is “filled” by several bias potentials over time, which allows larger barrier heights to be overcome. (Source: Pracht, Bohle, and Grimme 2020)

2.2.2.ORCA Quantum Chemistry Package

ORCA is an AB Initio, DFT and semiempirical SCF-MO package (Neese 2012). In this thesis, ORCA is used for the rest of the quantum chemical calculations. The optimization of structures obtained with CREST at the DFT level was carried out using the B3LYP (Becke 1993) functional with the def2-SVP (Weigend and Ahlrichs 2005) basis set, as the B3LYP functional has been observed to yield good results for BNN and similar two-dimensional materials in the literature (Lakshmy et al. 2023; Y. Liu et al. 2023; Ahmed et al. 2022; Hussain et al. 2018). Due to B3LYP functional′s particularly inaccurate calculation of non-covalent interaction energies, dispersion 4 (D4) (Caldeweyher et al. 2019) and geometrical counterpoise correction (gCP) (Kruse and Grimme 2012) were applied to all calculations. Geometrical counterpoise correction is required to compensate for basis set superposition errors (BSSE). Total electronic energy is calculated as:

$$E_{total} = E_{DFT} + E_{disp} + E_{gCP} \tag{2.3}$$

where E_{DFT} is the total energy of the DFT, E_{disp} is the dispersion correction energy energy and E_{gCP} is the geometrical counterpoise correction energy. Analytical frequency calculations were also carried out to confirm local minimum structures at the same level of theory.

2.3.Analysis Methods

As mentioned above, the calculations for the pristine BNN, doped-BNN and ion loaded BNN structures were carried out at B3LYP/def2-SVP/D4/gCP level of theory. The adsorption energy, ion capacity of per ion towards to the BNN surface is calculated as:

$$E_{ads} = E_{nM^{+}-host} - E_{host} - nE_{M^{+}} \tag{2.4}$$

where n is the number of adsorbed metal ions on the surface, $E_{nM^{+}-host}$ is the total electronic energy of the complex, E_{host} is the total electronic energy of the doped-BNN, $E_{nM^{+}}$ is the total electronic energy of the n number of isolated metal ion.

The specific capacity (C_C; current per unit mass) is calculated as:

$$C_C = \frac{nzF}{M_{nM^+-host}} \quad (2.5)$$

where z is the valency of the metal ion, F is the Faraday constant and M_{nM^+-host} is the molar mass of the complex. Finally, the voltage of the negative electrode material is calculated using Nerst equation:

$$V_{cell} = -\frac{\Delta G}{zF} \quad (2.6)$$

where the ΔG is calculated like E_{ads} in the equation 2.4 except total Gibbs free energy values are obtained from the analytic frequency calculations.

Structural parameters and molecular orbital diagrams are obtained with the aid of VMD (Humphrey, Dalke, and Schulten 1996) and Avogadro (Hanwell et al. 2012) packages.

Volume change per gram during the metal ion loading is calculated with Molovol package (Maglic and Lavendomme 2022) by using Van der Waals volumes with the equation:

$$\Delta V = V_f - V_i \quad (2.7)$$

where V_f is the Van der Waals volume of the optimized ion-loaded BNN structure without ions, V_i is the Van der Waals volume of the isolated optimized BNN structure.

2.4.Aim of the Study

The aim of this study is to examine whether BNN surfaces doped with Al, Cl, Co, Fe, Ga, O, P, and S atoms have the potential to be anode materials in K, Li, Mg, and Na ion batteries. Additionally, it seeks to clarify whether they could serve as alternatives to typical lithium batteries. The cationic radii of K, Li, Mg, and Na are approximately 152, 90, 86, and 116 pm, respectively. Smaller cationic radii can facilitate easier intercalation of ions and may result in smaller volume changes.

There are similar studies related to finding a suitable boron-nitride nanosheets as anode material for ion batteries (Jingyi Wu et al. 2020; Khan, Ahmad, and Ahmad 2021; Tapia et al. 2024). Likewise, dopants (Al, Cl, Co, Fe, Ga, O, P, S) were selected from the

similar studies present in the literature (Hosseinian et al. 2017). The anode behavior of BNN and doped BNN surfaces are rarely studied, and existing articles are quite new (Tyagi and Jaiswal 2022; Nazneen et al. 2023). Therefore, this study was initiated to explore new promising anode material based on 2D BNN nanosheets.

CHAPTER 3

RESULT AND DISCUSSION

3.1. Structures of Doped-BNNs

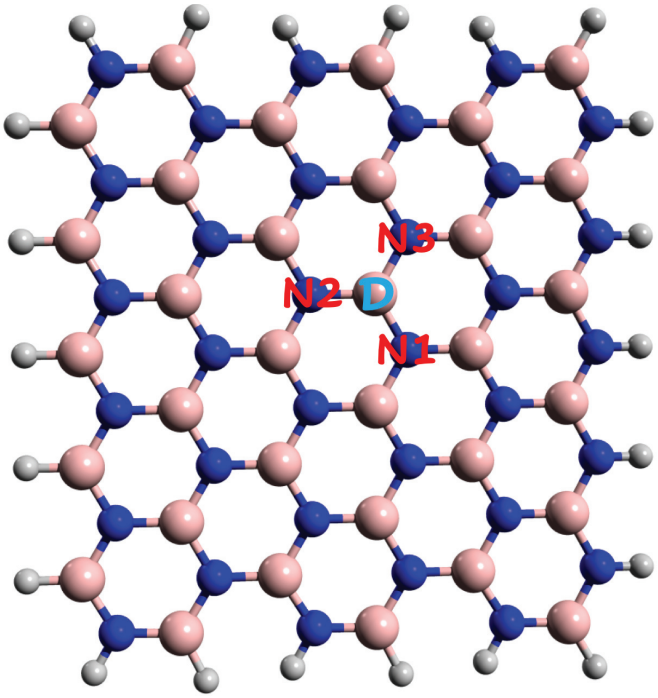

Figure 3.1. Optimized Boron-nitride nanosheet, dopant position (D) and nearest nitrogen atoms to the dopant (N1, N2, N3)

Electronic structure calculations primarily require a "good" starting structure of the molecule to be studied. In this study, a square-shaped hexagonal boron-nitride structure ($B_{33}N_{33}H_{22}$) was selected from the literature, and flawless geometry was created with Python code. In this code all distances between boron and nitrogen atoms were set to 1.45 Å, and the outer atoms were saturated with hydrogen atoms to minimize the boundary effect with , all distances between boron and nitrogen atoms were set to 1.45 Å, and the outer atoms were saturated with hydrogen atoms to minimize the boundary effect with a 1.09 Å distance for the initial structure. In this thesis, the dopant atoms (Al, Cl, Co, Fe, Ga, O, P, S) were placed at the position shown in Figure 3.1 (blue colored D

atom). The nearest nitrogen atoms to the dopant on the square-shaped hexagonal boron-nitride structure ($B_{33}N_{33}H_{22}$) are also shown in the Figure 3.1.

The effect of dopant atoms on the structure of BNN surface were examined by the bond distances between the dopant atom and nearest three nitrogen atoms (see Table 3.1). Depending on the bond order, Van der Waals radius of the dopant and interaction energies between the dopant and nitrogen atoms bond distances could change. Our results showed no unusual bond distances among all doped surfaces. Average bond distance of nitrogen-hydrogen is found as 1.02 Å, and average bond distance of boron-hydrogen is found 1.21 Å. Bond distance of boron and nitride atoms are found in agreement with the literature for the pristine BNN (Amorim et al. 2013). Therefore, it can be said that the performed optimization calculations are acceptable.

The dihedral angle, N1, N2, N3, D was measured for all BNN-nanosheets to compare the structure of the region around dopant with the same region in the pristine structure. This angle also shows how distant the dopant from the BNN surface. In pristine structure this angle is zero, it means the region is planar, and the dopant atom is in the BNN surface. The deviation from zero shows how far the dopant atom has moved away from the plane of the surface.

Table 3.1 Distances between the dopant and nearest nitrogen atoms in Å and dihedral angle of N1-N2-N3-D

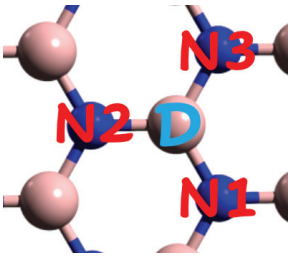

Structure Name	D-N1	D-N2	D-N3	Dihedral angle of N1-N2-N3-D
Pristine BNN	1.451	1.455	1.451	0.0
Al-doped BNN	1.733	1.737	1.734	18.5
Cl-doped BNN	1.957	1.695	1.949	1.1
Co-doped BNN	1.764	1.768	1.764	44.0
Fe-doped BNN	1.782	1.789	1.783	44.0
Ga-doped BNN	1.780	1.784	1.781	21.5
O-doped BNN	1.430	1.430	2.360	35.0
P-doped BNN	1.735	1.741	1.737	46.9
S-doped BNN	1.697	2.187	1.697	44.8

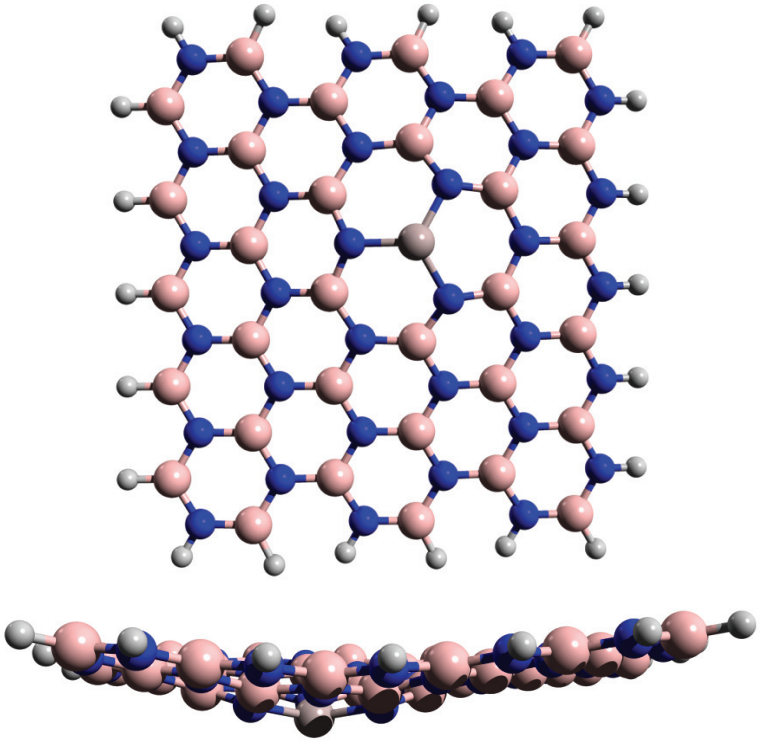

Figure 3.2. Top view and side view of optimized Al-doped BNN structure

The planarity of the BNN is disturbed by the aluminum doping; the overall structure of surface changed significantly, and it shows concave-like geometry (see Figure 3.2). The three closest hexagonal holes to D atom became more wider with the introduction of aluminum. Dihedral angle of N1-N2-N3-Al is 18.5°, so that it slightly moved away from the center of the surface. Since aluminum is trivalent and it has 3 electrons in the outer shell, it's able to bond with the surrounding nitrogen atoms, the N-Al bond distance is found as 1.73 Å.

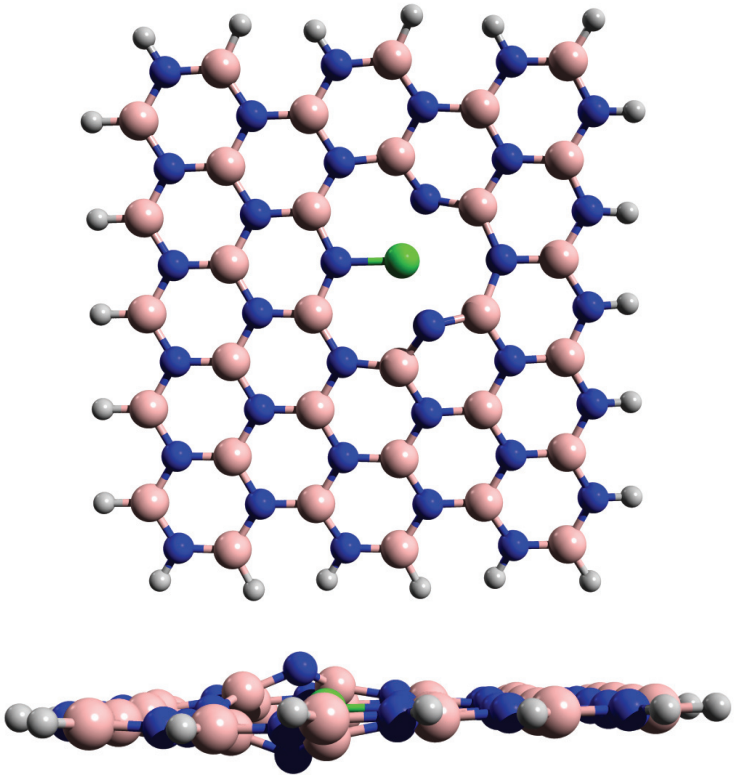

Figure 3.3. Top view and side view of optimized Cl-doped BNN structure

Chlorine doping significantly changes the geometry because chlorine atom cannot form three bonds but can only form one bond (1.70 Å) (see Figure 3.3). The lone pair electrons on the chlorine and on the nitrogens that do not bound with the chlorine repel each other (the distance is about 1.95 Å).. This is why it locally changes the geometry rather than completely, and the part that remains distant maintains planarity. The position of the chlorine itself is almost same and the dihedral angle of N1-N2-N3-Cl is 1.1°.

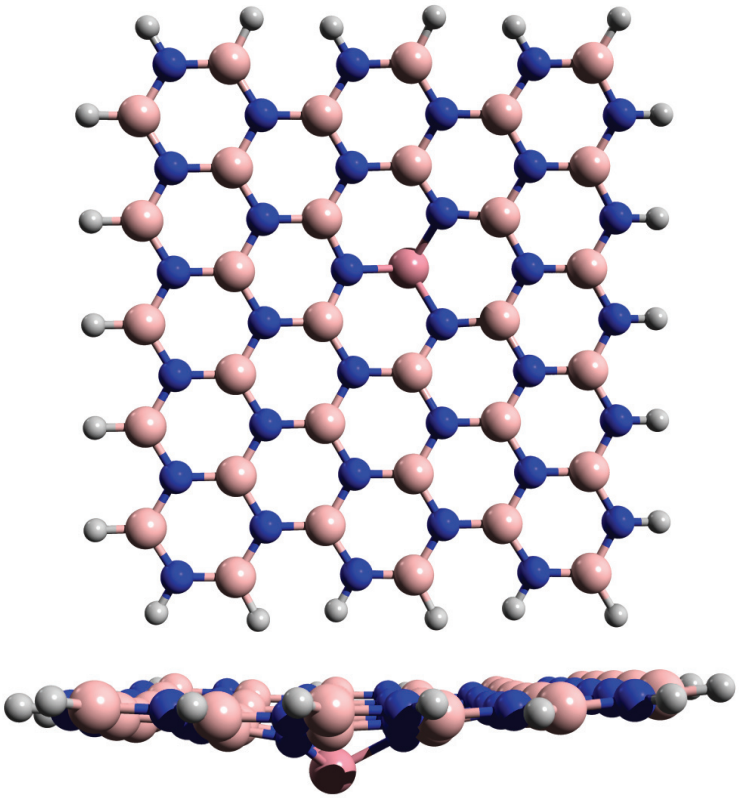

Figure 3.4. Top view and side view of optimized Co-doped BNN structure

The coordination number of cobalt could be up to six. It makes three bond in the Co-doped BNN structure (see Figure 3.4), and average bond distance between the cobalt and nitrogens is about 1.765 Å. Cobalt doping caused a slight change on the planarity of boron-nitride field, but it broke the planarity during optimization and moved out of the surface. Thus, the dihedral angle of N1-N2-N3-Co is large with the value of 44°. The size of the closest three hexagonal holes to the cobalt did not change meaningfully.

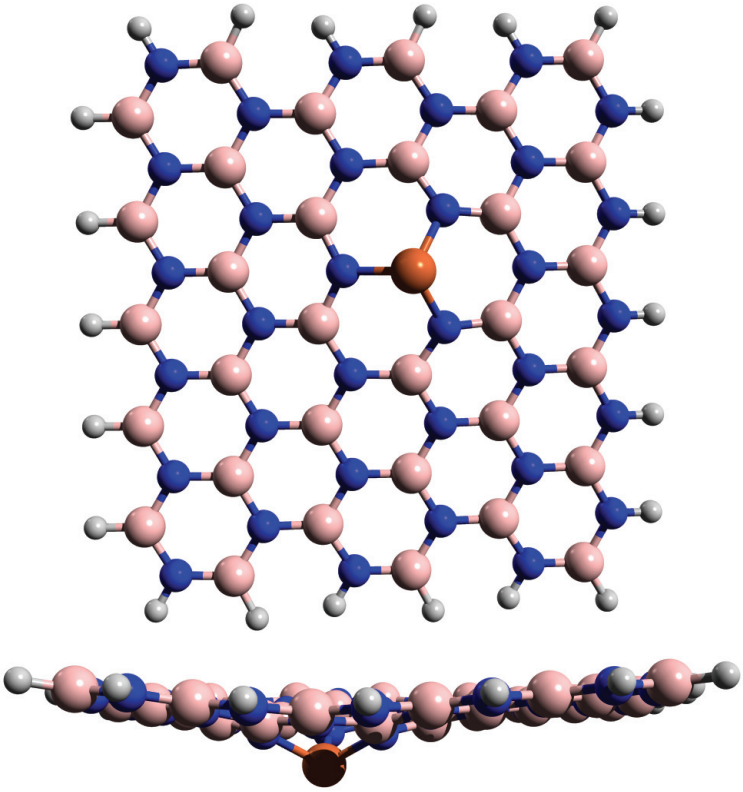

Figure 3.5. Top view and side view of optimized Fe-doped BNN structure

The structure of the Fe-doped BNN surface is given in Figure 3.5. The structural change in the Fe-doped BNN surface is similar to that of the Al-doped BNN, with slightly less disruption to planarity and the formation of concave-like geometry as well. It still manages to form three bonds with an average bond distance of about 1.785 Å. As depicted in Figure 3.5, two of the three hexagonal holes closest to the iron retain their hexagonal structure while one of them exhibits a slight structural disturbance. However, iron itself is largely repelled from the surface, just as cobalt is. The dihedral angle N1-N2-N3-D is 44° for both.

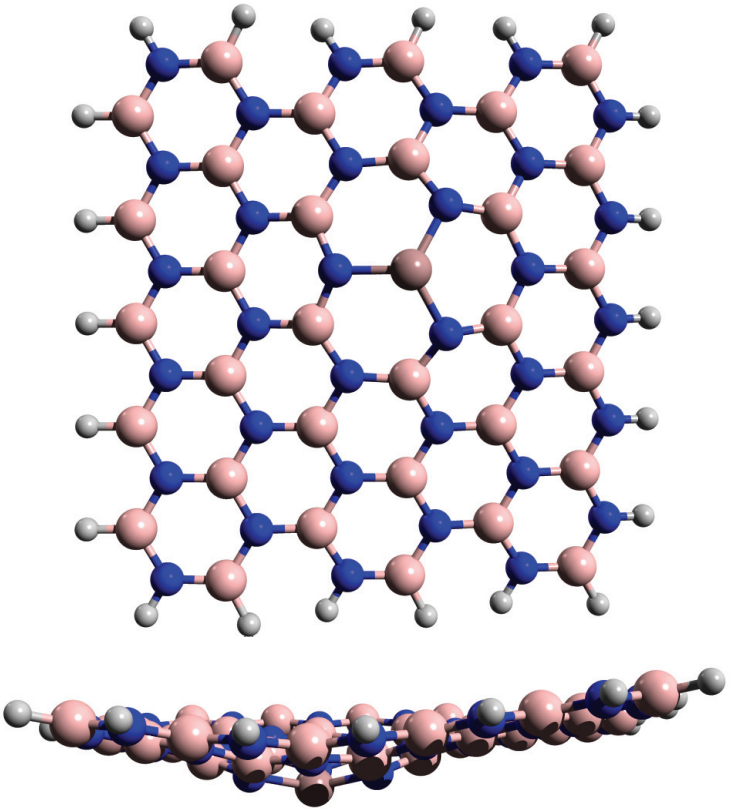

Figure 3.6. Top view and side view of optimized Ga-doped BNN structure

Gallium forms compounds primarily in the 3+ oxidation state such as gallium-nitride. Therefore, it can form three bonds in the BNN structure. The average bond distances between the gallium and N1, N2, N3 are about 1.782 Å, and the dihedral angle of N1-N2-N3-Ga is 21.5°. The structural change in the Ga-doped BNN is almost similar with the Al-doped BNN (see Figure 3.6). Both disturbed the planarity of BNN surface and formed concave-like geometry.

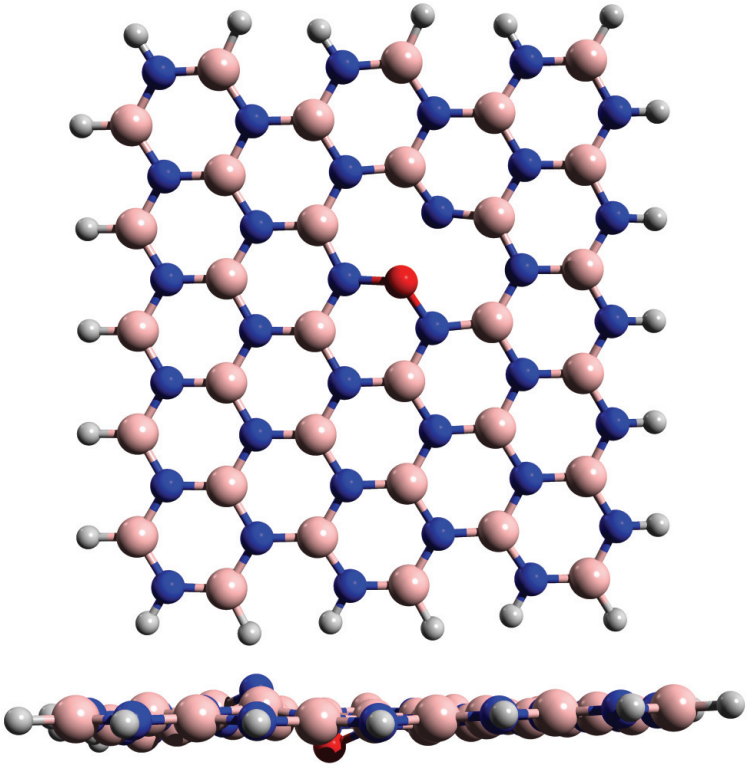

Figure 3.7. Top view and side view of optimized O-doped BNN structure

Structural changes in the O-doped BNN structure is similar to the Cl-doped BNN. Oxygen has a bond length of 1.430 Å with N1 and N2, while the distance with N3 is 2.360 Å, and the dihedral angle of N1-N2-N3-O is 35°. Chlorine formed one covalent bond with nitrogen atom and has three lone pairs, oxygen formed two bonds with N-atom around it with one remaining lone pair on it. For this reason, it can be said that the repulsive force between oxygen and nitrogen is lower, and so oxygen does not have a bond with one of the N atoms near to it. Also, the planarity of the structure is almost not affected (see Figure 3.7).

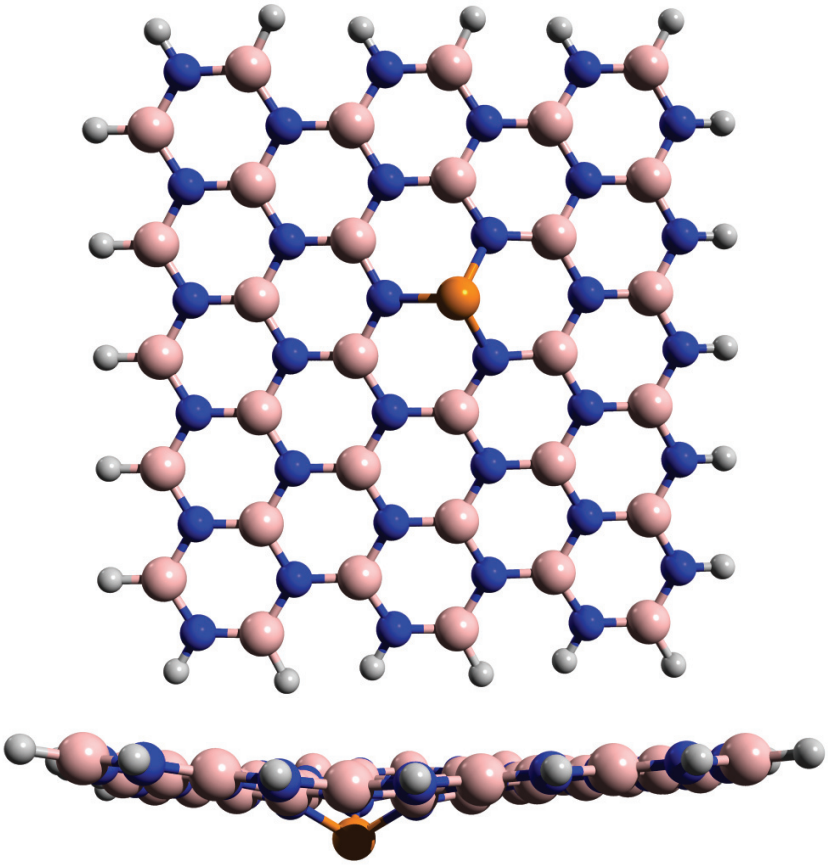

Figure 3.8. Top view and side view of optimized P-doped BNN structure

Phosphorus formed bonds with three nitrogen atoms with an average bond distance of 1.738 Å. The phosphorus doping did not change the planarity of the structure too much, it just caused a slightly concave geometry. Dopant is repelled from the center due to the lone pair, which creates a defect site. The dihedral angle of N1-N2-N3-P confirms this with a value of 46.9°.

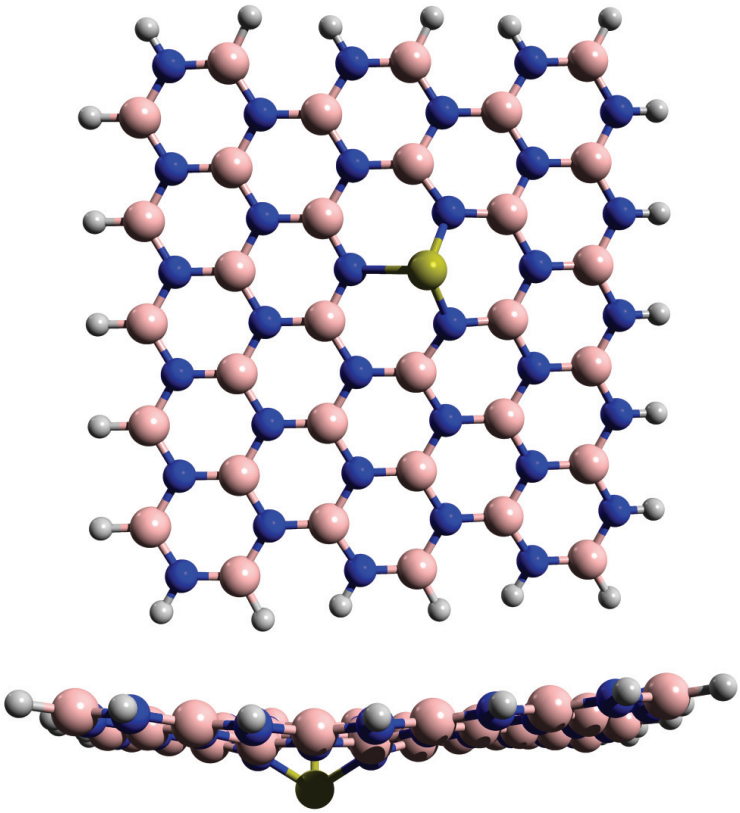

Figure 3.9. Top view and side view of optimized S-doped BNN structure

The structural change in the S-doped BNN structure is given in Figure 3.9, it is similar that of Fe-doped BNN. It almost preserves the planarity on the boron-nitride field. However, the sulfur is repelled from the center, and the symmetry is broken. Thus, the dihedral angle of N1-N2-N3-S has a large value of 44.8°. The bond formation between the sulfur and nitrogen is not clear as the others. The distance between the two of three nitrogen and sulfur is about 1.697 Å and for the last one 2.187 Å. Therefore, two hexagonal holes have shrunk while one has expanded.

3.2.Electronic Structure of Doped-BNNs

Analysis of the electronic structure of the doped-BNNs could give an idea about the conductivity, band gap, orbital compositions, and charge transfer states. According to our calculations HOMO-LUMO gap of the boron-nitride nanosheet is about 5.89 eV at B3LYP/def2-SVP/D4/gCP level of theory. This agrees with the measurements of single crystal of hexagonal boron-nitride, which has a band gap energy of 5.77 eV (Watanabe, Taniguchi, and Kanda 2004). The difference from the experimental data is only 0.12 eV. Benchmark studies of the HOMO-LUMO gap energies, including B3LYP, show much larger deviations from the reference values. Even mean absolute error of machine learning boosted B3LYP HOMO-LUMO gap energies are around 0.15 eV (Zhang and Musgrave 2007; Pereira et al. 2017). Therefore, we can say that the chosen method is highly accurate for the corresponding pristine structure. However, there are no reference values for doped-BNNs and ion-introduced structures as they are not included in the literature.

Table 3.2 HOMO-LUMO energies, energy gap of the pristine BNN and doped-BNNs, and percent change in the energy gap with respect to the pristine BNN.

Structure Name	HOMO (eV)	LUMO (eV)	Energy Gap (eV)	%ΔEg
BNN	-6.42	-0.53	5.89	-
Al-doped BNN	-6.39	-0.75	5.64	4.17
Cl-doped BNN	-5.34	-0.99	4.35	26.13
Co-doped BNN	-6.17	-2.36	3.80	35.35
Fe-doped BNN	-6.07	-2.20	3.87	34.16
Ga-doped BNN	-6.39	-1.12	5.27	10.48
O-doped BNN	-5.95	-0.58	5.38	8.65
P-doped BNN	-5.69	-0.54	5.15	12.52
S-doped BNN	-4.74	-0.41	4.33	26.43

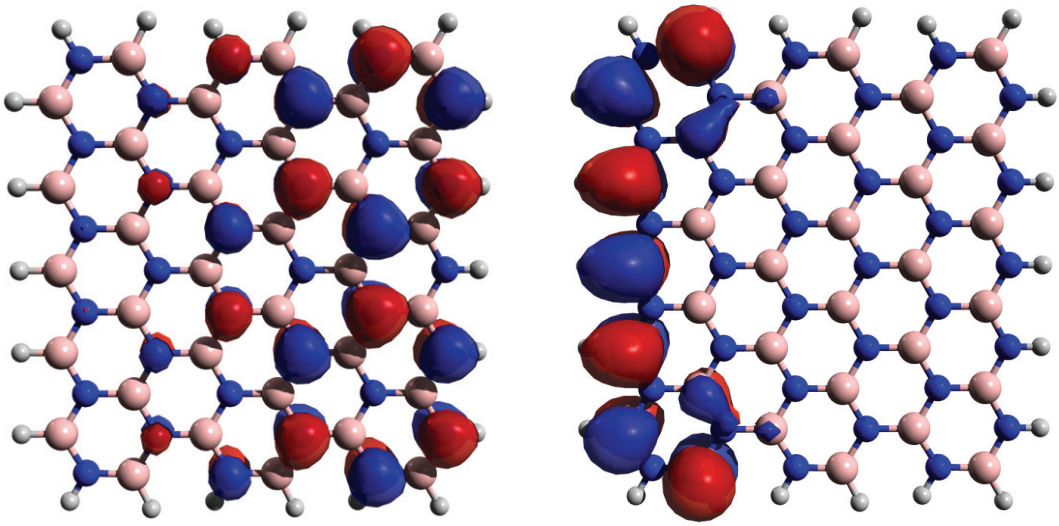

HOMO LUMO

Figure 3.10. HOMO, LUMO orbitals of pristine BNN

The HOMO and LUMO structures of pristine BNN nanosheet given in Figure 3.10 shows an intra-molecular charge transfer within the pristine BNN. The HOMO electron density is localized on the lone pairs of nitrogen atoms, while the LUMO electron density is found only on the lone pairs of boron atoms at the other edge. The nonbonding p orbitals of nitrogen atoms act as acceptors, and the p orbitals of boron atoms serve as donors. This is also confirmed by the molecular orbital (MO) coefficients of boron and nitrogen atoms at the HOMO and LUMO levels. The highest MO coefficient value correspond to the the nitrogen atoms is p orbital at the HOMO level, and p orbital at the LUMO level for the boron atoms.

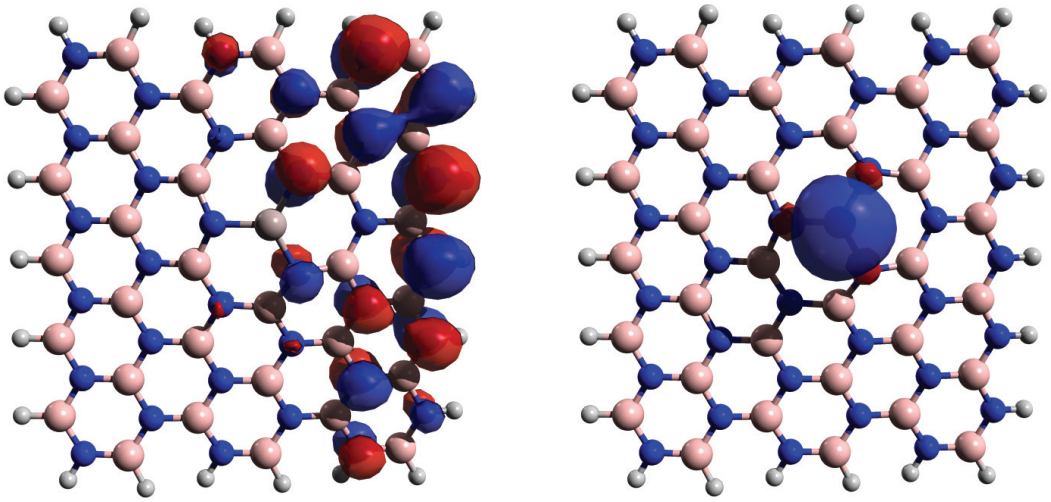

HOMO LUMO

Figure 3.11. HOMO, LUMO orbitals of Al-doped BNN

As shown in Figure 3.11, there is a charge transfer between the aluminum and the lone pairs of nitrogen atoms. Aluminum acts as a good acceptor, with electron density primarily gathered on it at the LUMO, which has an s orbital character primarily for Al-doped BNN. Meanwhile, the nonbonding p orbitals of nitrogen act as donors to the aluminum. The HOMO-LUMO gap energy was reduced by only 4.17%, indicating that the conductivity was not significantly affected by the Al-doping.

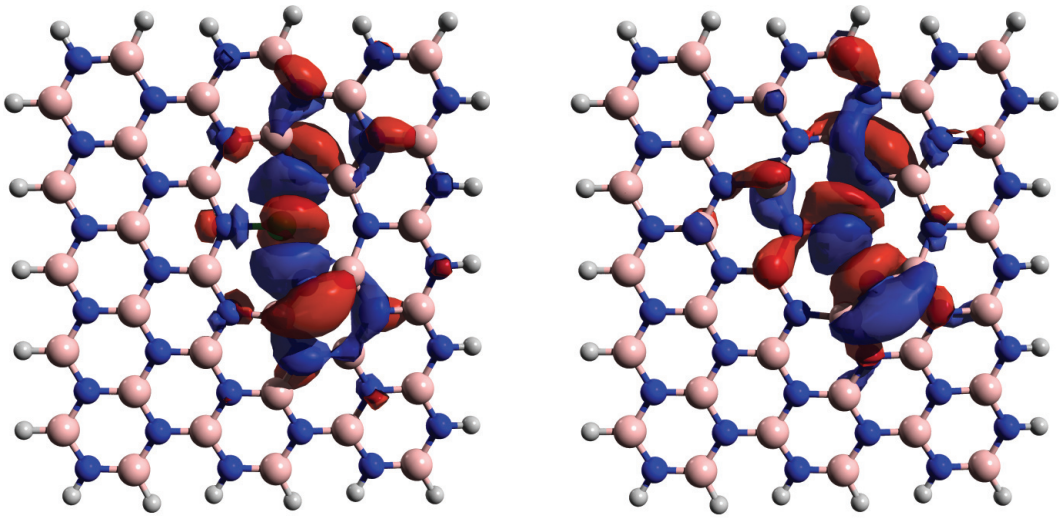

HOMO LUMO

Figure 3.12. HOMO, LUMO orbitals of Cl-doped BNN

The Cl-doped BNN material does not exhibit charge transfer properties (see Figure 3.12). The HOMO-LUMO orbitals are localized in the same region, consisting of a mixture of s and p orbitals of boron, nitride, and chlorine. This mixture applies to the LUMO as well. The MO contributions from the chlorine significantly higher in the LUMO. The HOMO-LUMO gap energy of Cl-doped BNN is approximately 4.35 eV, which is 26.13% less than pristine BNN. Therefore, chlorine doping has notably increased the conductivity.

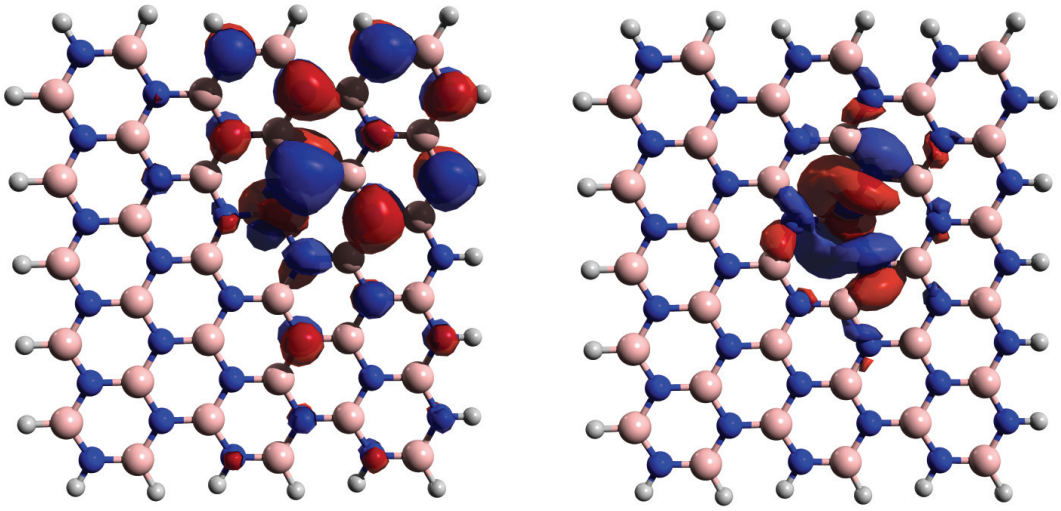

HOMO LUMO

Figure 3.13. HOMO, LUMO orbitals of Co-doped BNN

The MO composition of HOMO of Co-doped BNN is similar to the HOMO of pristine BNN, but electron density is less. Cobalt includes mixtures of p and d orbitals at both the HOMO and LUMO levels, and there is no electron transfer between the two energy levels. The energy gap of Co-doped BNN was found to be 3.80 eV, which means it is 35.35% lower compared to the pristine structure. The doping effect considerably increased conductivity.

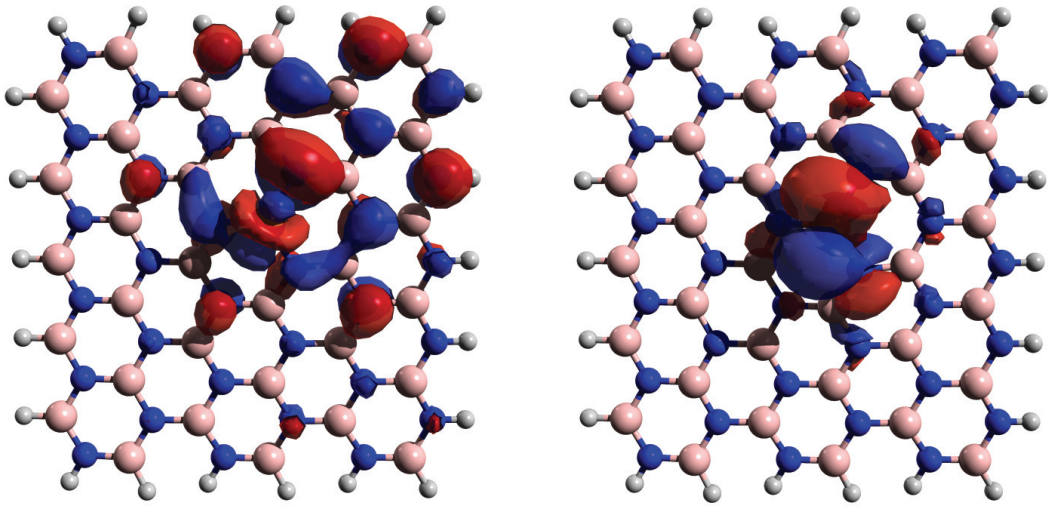

HOMO LUMO

Figure 3.14. HOMO, LUMO orbitals of Fe-doped-BNN

The effects of iron and cobalt, which are transition metals consecutively located in the periodic table, on the electronic structure of boron-nitride are unsurprisingly similar to each other. Even the energy gap is almost the same, at 3.87 eV. This means that iron doping increased conductivity by 34.16%. Even if there is no electron transfer in the structure, the migration of electrons from the non-bonding p orbitals of the nitrogen atom to the p orbital of iron is observed.

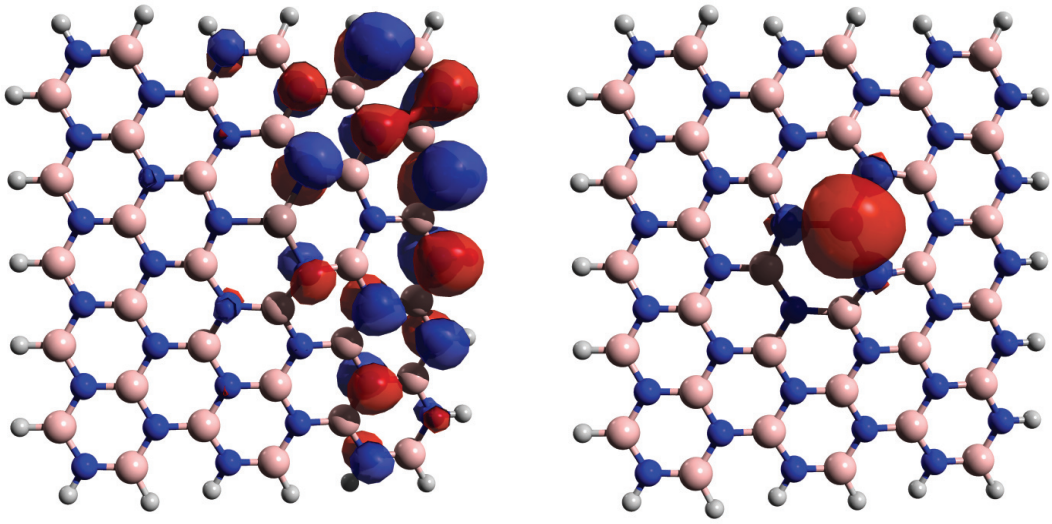

HOMO LUMO

Figure 3.15. HOMO, LUMO orbitals of Ga-doped BNN

According to Figure 3.15, there is no electron density on gallium in the HOMO structure. According to the MO coefficients, gallium's s orbital is very dominant at the LUMO structure. There is a charge transfer from the non-bonding p orbitals of nitrogens to the s orbital of gallium between HOMO and LUMO. The HOMO-LUMO gap energy was found to be 5.27 eV, and the conductivity increased by approximately 10%.

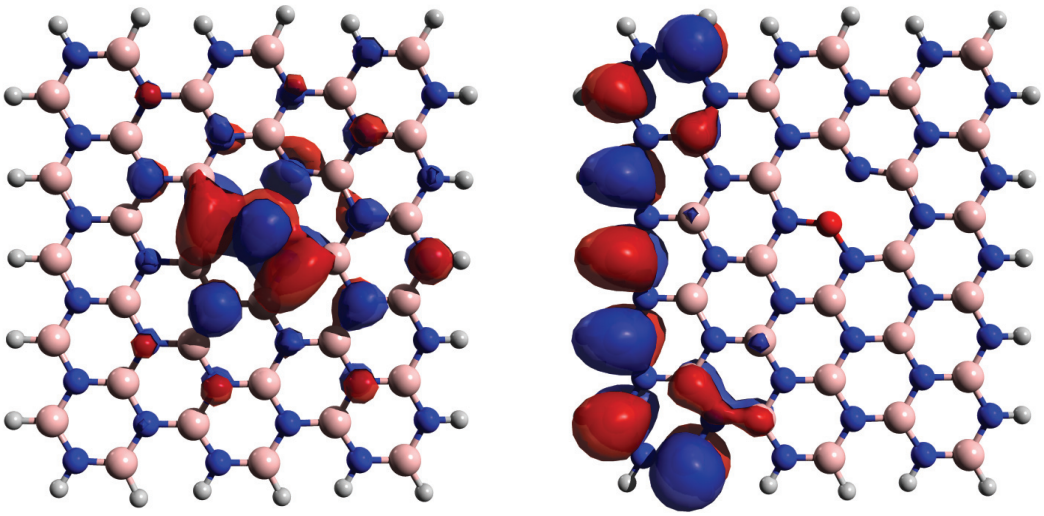

HOMO LUMO

Figure 3.16. HOMO, LUMO orbitals of O-doped BNN

Figure 3.16 present a clear charge transfer in the O-doped BNN structure as well. However, unlike in Al-doped BNN and Ga-doped BNN, while the electron density in the HOMO is localized on the dopant, the LUMO does not host, so oxygen is acting as an electron donor. The electron density in the LUMO is very similar to that of the pristine structure. While the contributions of both oxygen′s and nitrogen′s p orbitals are observed in the HOMO, only the contributions of the boron atoms' p orbitals are present in the LUMO. The conductivity of the structure has decreased by only 8.65%.

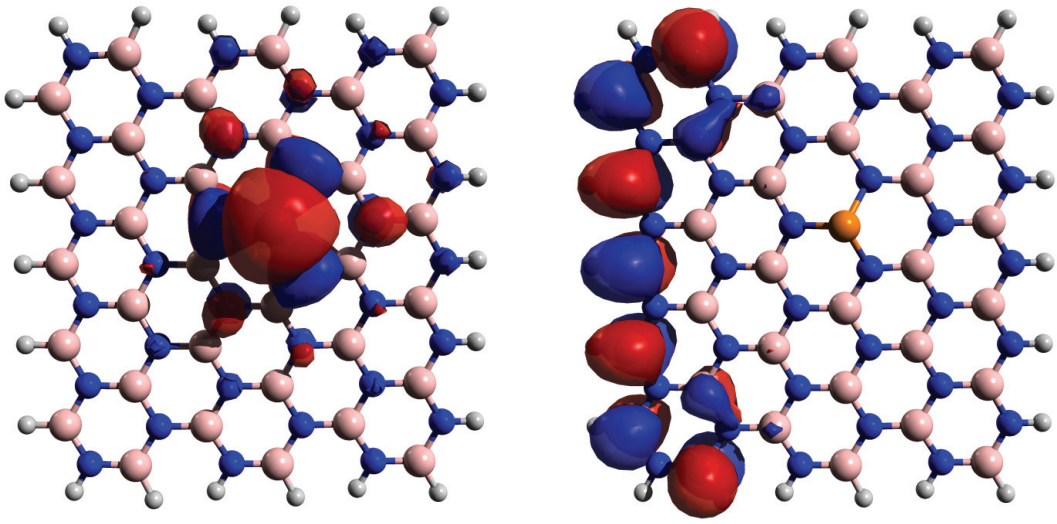

HOMO LUMO

Figure 3.17. HOMO, LUMO orbitals of P-doped BNN

The effect of phosphorus doping on the electronic structure is similar to that of oxygen doping (Figure 3.17). The s and p orbitals of phosphorus atom contributed highly to HOMO. However, electron density is localized on the p orbitals of boron atoms at the LUMO. Dopant, N1, N2 and N3 atoms act as donors and boron atoms act as an acceptor, which shows charge transfer property. HOMO is mainly consist of mixture of s and p orbitals of phosphorus. The HOMO-LUMO gap energy was found to be 5.15 eV, and the conductivity increased by approximately 13%.

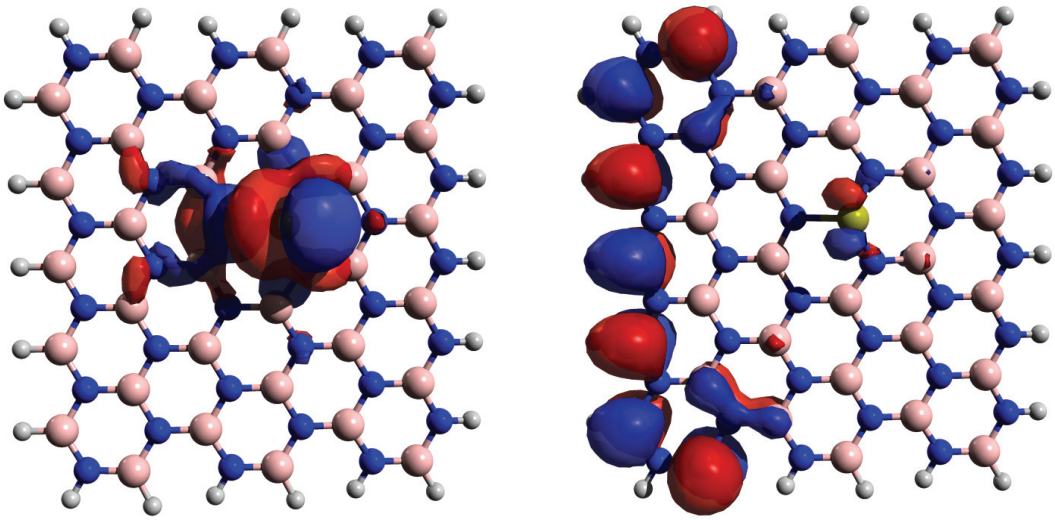

Figure 3.18. HOMO, LUMO orbitals of S-doped BNN

The similar electronic structures of oxygen, phosphorus, and sulfur, being nonmetals, affect their electronic structures in a similar manner. In fact, the impact of oxygen and sulfur, both in group 6A, on the HOMO-LUMO levels is nearly identical. However, sulfur contributes to conductivity much better than oxygen due to its higher number of valence electrons. The energy gap is 4.33 eV, which has dropped by about 26% compared to the pristine structure. The largest contribution to the HOMO comes from sulfur's nonbonding p orbitals, yet at the LUMO where the electron density on sulfur remains very small. This indicates a charge transfer from sulfur to boron atoms at the one edge of BNN. Electron density at the LUMO level is present only in the p_x orbital of boron.

3.3.Anode Material Capability

The capability of doped boron-nitride as an anode material is the main subject of this work. For this purpose, the maximum ion transport capacity is determined by examining each structure individually. Ions: K, Li, Mg and Na were added sequentially to the optimized doped BNN structures, and the number of ions was increased one by one. If an ion was added to the top surface of the structure, the next one was added to the bottom surface to ensure balance. All results of single ion addition were reported, even

for the non-favorable ones. Cases, where ions did not adhere to the surface were not included in the results section due to the non-converged optimization. Maximum ion transport capacities are shown in Figures 19-26. Adsorption energies, voltage of the corresponding negative electrode material, and theoretical specific capacities were calculated.

The motion of the ions on the doped BNN surface is important for conductivity. However, if a covalent bond forms between the ion and the surface, ion transportation is not possible. It is similar to the formation of dendrites. Such situations not only shorten the battery life but also has a safety risk. For Al-doped BNN, it was observed that the structure is not suitable for magnesium-ion batteries because the magnesium ion comes very close to aluminum and forms a covalent bond with the anode surface (see Figure 3.19). For lithium-ion battery it could hold up to three ions, and it has the best theoretical specific capacity as 193 mAh/g. However, since the adsorption energy has a positive value (0.32 kcal/mol), it seems unlikely to stably retain ions on the surface. Even when we accept DFT's margin of error as 0.3 eV (6.9 kcal/mol), the possibility of this structure being favorable still exists. However, looking at the voltage of the material, we can more clearly see it is not favorable with a value of -1.19 eV. The negative value of the cell voltage indicates that this system cannot be used practically in a battery. A negative potential difference indicates that, the flow of electrons from the anode to the cathode is not spontaneous and so the battery will not produce electricity. When we look at the results for potassium and sodium batteries, we see that the BNN surface has a maximum ion transport capacity of 2 ions.

The voltage of the negative electrode material and adsorption energies are favorable for all these structures. Voltage values vary between 0.39 and 1.39 V, which falls within the desirable range. In a typical battery, it is preferred for the voltage of the negative electrode material to be between 0 and 2 volts (Landi et al. 2009). Otherwise, a situation known as plating can occur on the anode. This can significantly degrade battery performance and cycle life, and increase the risk of short-circuiting and thermal runaway, leading to safety hazards. Results of the theoretical specific capacity showed that the structure with 2 potassium ions has 113.25 mAh/g, while the structure containing 2 sodium ions has 127.80 mAh/g. For reference, in classic lithium batteries, this value is approximately 372 mAh/g (Tarascon and Armand 2001).

Another important parameter is the volumetric change in the doped-BNN structure with ion loading. This theoretical volume was calculated using Van der Waals

volumes. In the calculation, ions loaded onto the surface were removed, and only the volume of the surface was examined in its initial and final states. Having different volumes of battery in charged and discharged states is not a desired characteristic and can pose a safety vulnerability. The highest volumetric change was found to be 26.40 cm^3 for magnesium ion and 13.54 cm^3 for three lithium ions per 100 grams of material, respectively. For the other ions, this value was observed below 10 cm^3.

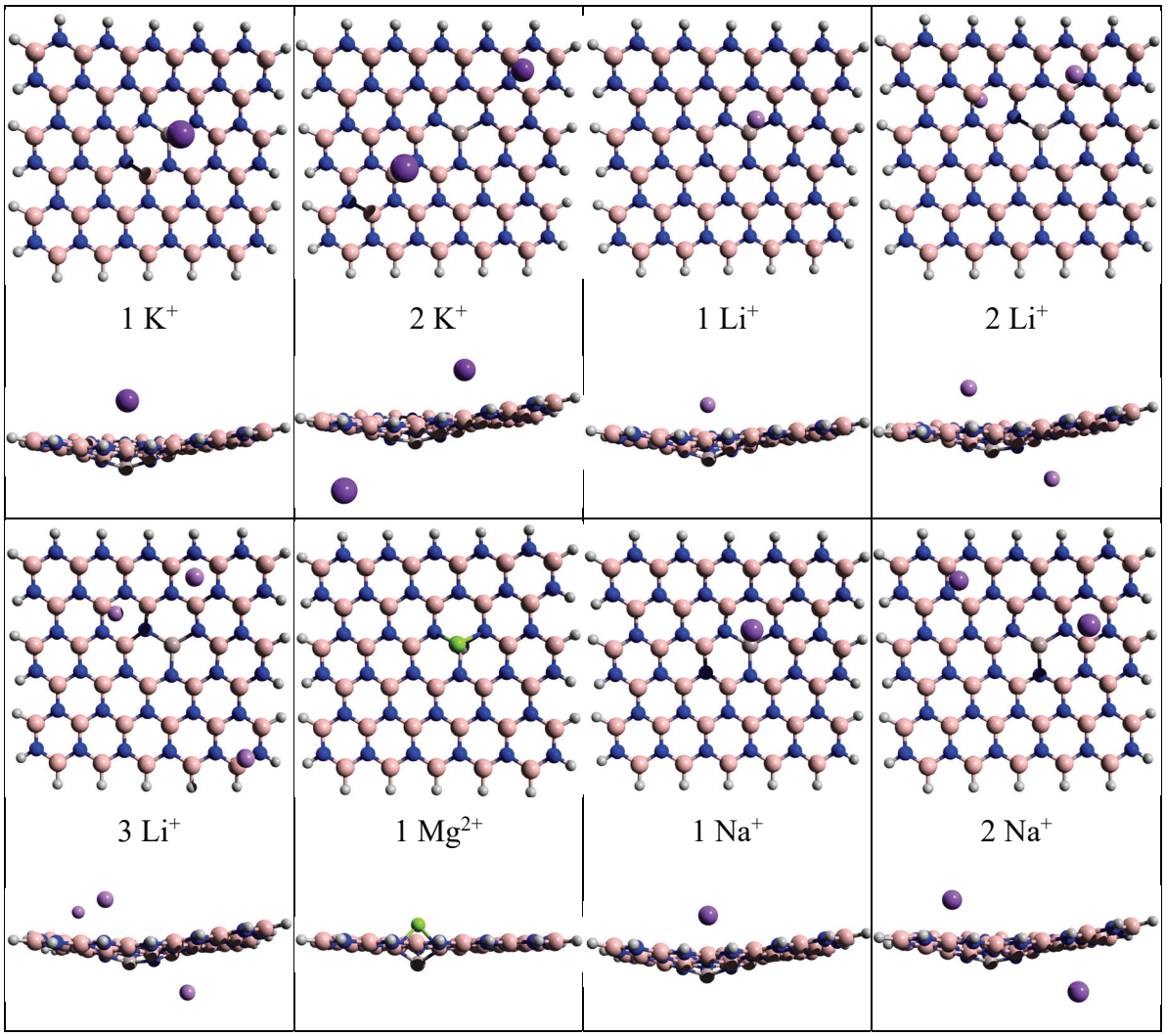

Figure 3.19. Optimized structure of ion loaded top and side view of Al-doped BNN

Table 3.3. Adsorption energy (E_{ads}), voltage of the corresponding negative electrode material (V_{cell}), theoretical specific capacity (C_c) and theoretical volume change between the charged and discharged states (ΔV) for 100 g of material of Al-doped BNN

Name	E_{ads} (kcal/mol)	V_{cell} (V)	C_c(mAh/g)	ΔV (cm^3)
Al-BNN + K^+	-33.17	1.06	61.72	5.87
Al-BNN + $2K^+$	-26.29	0.39	113.25	3.91
Al-BNN + Li^+	-41.23	1.39	66.66	6.88
Al-BNN + $2Li^+$	-38.94	0.88	131.06	7.73
Al-BNN + $3Li^+$	0.32	-1.19	193.31	13.54
Al-BNN + Mg^{2+}	-199.47	8.16	127.80	26.40
Al-BNN + Na^+	-37.20	1.23	64.10	5.94
Al-BNN + $2Na^+$	-33.21	0.67	121.52	6.72

In the chlorine-doped BNN structure, all structures are thermodynamically stable and can adhere to the surface (see Figure 3.20). However, we see that this structure is not suitable for magnesium ion and lithium-ion batteries. Both ions bound to the surface with a covalent bond. This situation can be understood when looking at the adsorption energies. The adsorption energies for lithium and magnesium are quite high, at 117.90 kcal/mol and 278.81 kcal/mol, respectively (see Table 3.4). This could make ion transportation impossible. When looking at potassium and sodium ions, it was observed that they have a maximum capacity of 2 ions. In this example, the maximum capacity voltage was observed to be 2.57 V for potassium and 2.54 V for sodium. Since the voltage of the anode material being this high is not a desired situation, this material is not expected to yield good results in practical applications. By analyzing the theoretical specific capacities, we see that it is 111.26 mAh/g for potassium batteries, while for sodium batteries, it is a maximum of 119.23 mAh/g. Examining the volume changes for 100 grams of material, we again see that the structures bonded with covalent bonds, significantly change the surface's bond/dihedral angles, hence also altering the volume significantly. This value is approximately 24 cm^3 for magnesium, while it is 15.44 cm^3 for lithium. For the remaining BNN structures, it was observed that there are volumetric changes in the range of approximately 12.06-15.61 cm^3 between charged and discharged states.

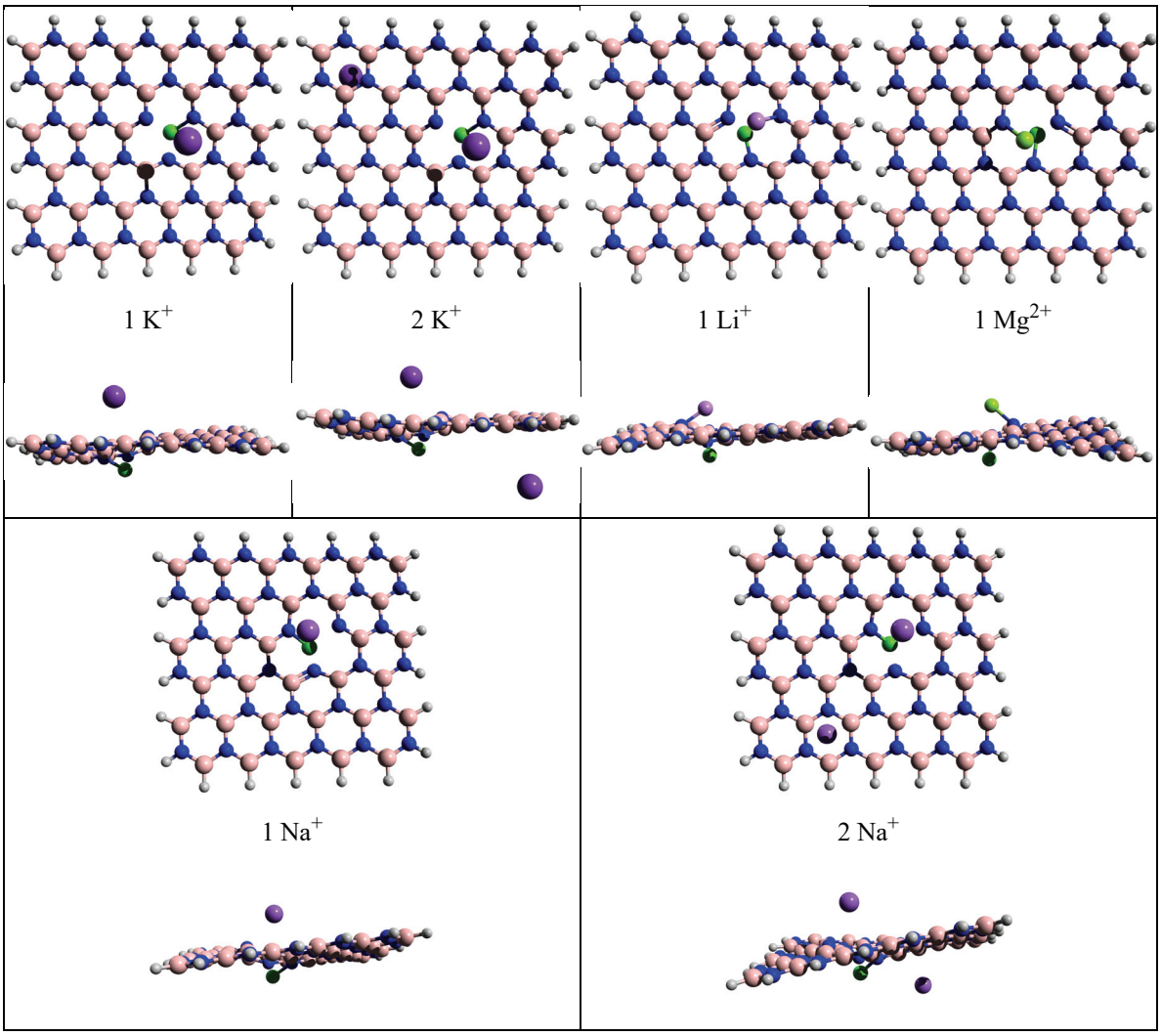

Figure 3.20. Optimized structure of ion loaded top and side view of Cl-doped BNN

Table 3.4. Adsorption energy (E_{ads}), voltage of the corresponding negative electrode material (V_{cell}), theoretical specific capacity (C_c) and theoretical volume change between the charged and discharged states (ΔV) for 100 g of material of Cl-doped BNN

Name	E_{ads} (kcal/mol)	V_{cell} (V)	C_c(mAh/g)	ΔV (cm^3)
Cl-BNN + K^+	-80.41	3.03	60.54	12.06
Cl-BNN + $2K^+$	-78.77	2.57	111.26	14.44
Cl-BNN + Li^+	-117.90	4.59	65.29	15.44
Cl-BNN + Mg^{2+}	-278.81	11.62	125.27	23.99
Cl-BNN + Na^+	-92.04	3.55	62.83	13.13
Cl-BNN + $2Na^+$	-77.14	2.54	119.23	15.61

The tendency of magnesium ions to form covalent bonds is also valid within Co-doped BNN. In fact, as seen in Figure 3.21, the magnesium ion has almost pushed cobalt out of the structure and has settled itself in place. The fact that the magnesium ion has a 2+ charge and the presence of magnesium nitride among the compounds it forms with nitrogen, indicating a propensity for this bond formation, could be causing magnesium to yield poor results. As seen in Table 3.5, magnesium is bonded to the surface with a high energy of 235.80 kcal/mol. Looking at the results in general, the ion capacity does not exceed 2. The theoretical specific capacity for these structures varies between 106.09 mAh/g and 121.56 mAh/g. Unfortunately, even with the Co-doped BNN structure, the energy density typical of lithium batteries could not be achieved theoretically. The cell voltage, however, varies exactly within the sought range, between 0.10 V and 2.00 V. We can confirm here that high voltage leads to plating. Upon examining the structure containing magnesium, we observe a voltage of 9.77, which causes undesirable results. The Van der Waals volume difference also possesses a desirably low value, varying between 2.26 cm^3 and 7.75 cm^3 for 100 grams of material. As also seen in Figure 3.21, when examining the optimized structures, no significant changes are observed in the structure with ion loading.

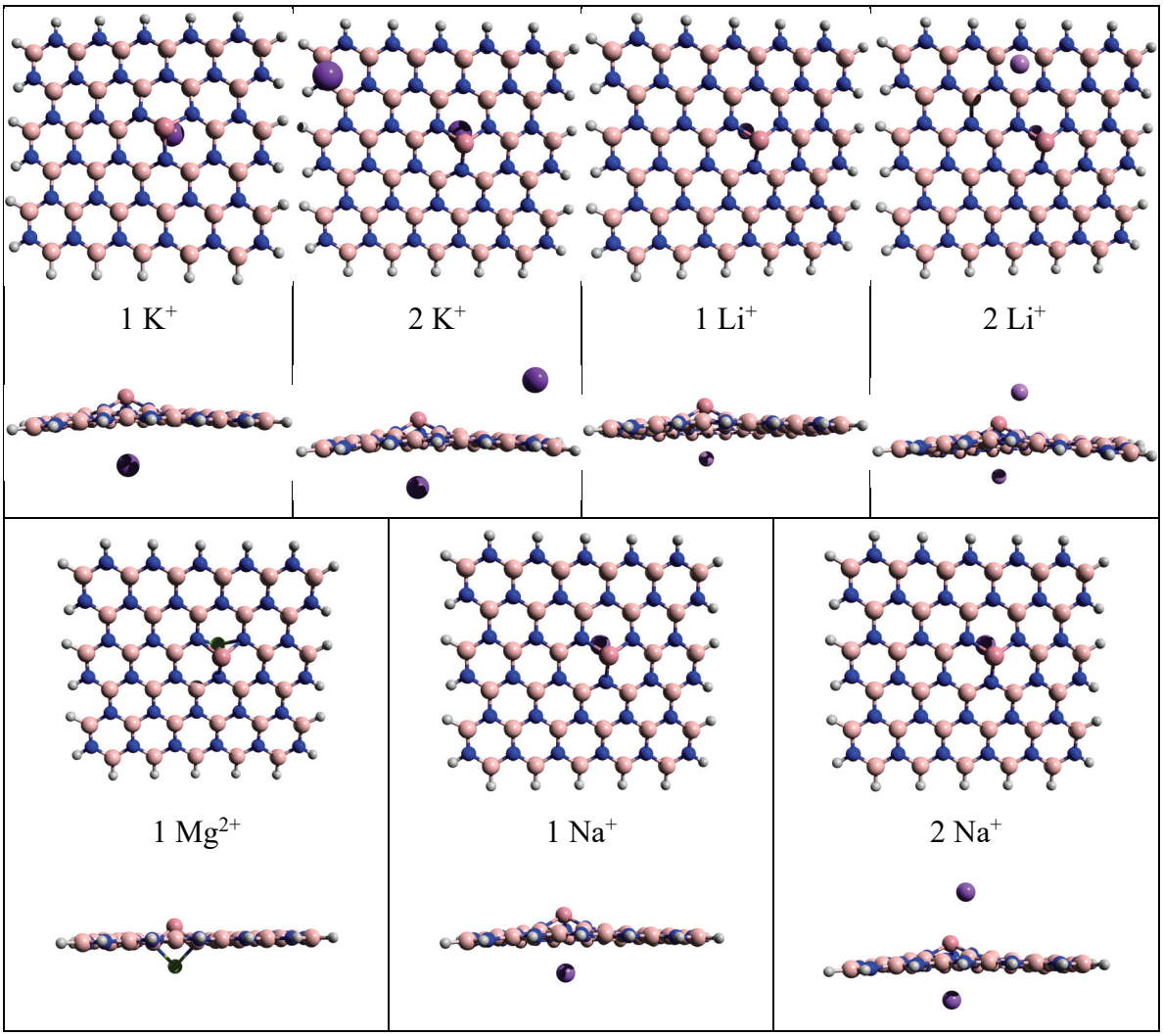

Figure 3.21. Optimized structure of ion loaded top and side view of Co-doped BNN

Table 3.5. Adsorption energy (E_{ads}), voltage of the corresponding negative electrode material (V_{cell}), theoretical specific capacity (C_c) and theoretical volume change between the charged and discharged states (ΔV) for 100 g of material of Co-doped BNN

Name	E_{ads} (kcal/mol)	V_{cell} (V)	C_c(mAh/g)	ΔV (cm^3)
Co-BNN + K^+	-42.13	1.41	57.49	3.23
Co-BNN + $2K^+$	-33.92	0.73	106.09	4.94
Co-BNN + Li^+	-56.47	2.00	61.75	4.65
Co-BNN + $2Li^+$	-47.19	1.29	121.56	7.75
Co-BNN + Mg^{2+}	-235.80	9.77	118.76	7.28
Co-BNN + Na^+	-49.47	1.73	59.55	3.98
Co-BNN + $2Na^{2+}$	-19.26	0.10	113.31	2.26

When we loaded ions onto the BNN structure under the influence of iron, interesting results were obtained. Magnesium ion loading does not lead to the formation of a covalent bond (see Figure 3.22). The theoretical specific capacity is high, 226.85 mAh/g, due to magnesium's 2+ charge. However, when looking at the voltage values, very high results was seen (see Table 3.6). This is not a desired outcome and may hinder practical use. Another interesting result regarding magnesium is that volume contraction, not volume expansion, is observed when one ion is added with the value of -1.78 cm^3. Examining other ions, the possibility of this structure being suitable for potassium or sodium ion batteries is quite low. The maximum number of ions that potassium and sodium can hold remained at 1. Therefore, a low energy density of approximately 58 mAh/g was observed for both. Even if the energy capacities are not high, the effects of potassium and sodium ions on the change in volume and voltage values are within the desired range. The results are better for lithium-ion batteries. The structure could be optimized with a maximum of 3 ions, but when there are 3 ions, the adsorption energy and voltage value do not seem to be at desired levels. In cases where it holds 2 lithium ions, the voltage value is 1.14 V, and the change in volume for 100 grams is 7.10 cm^3, both of which are at a desirable level. However, the energy capacity is significantly lower than typical lithium batteries, at 122.42 mAh/g.

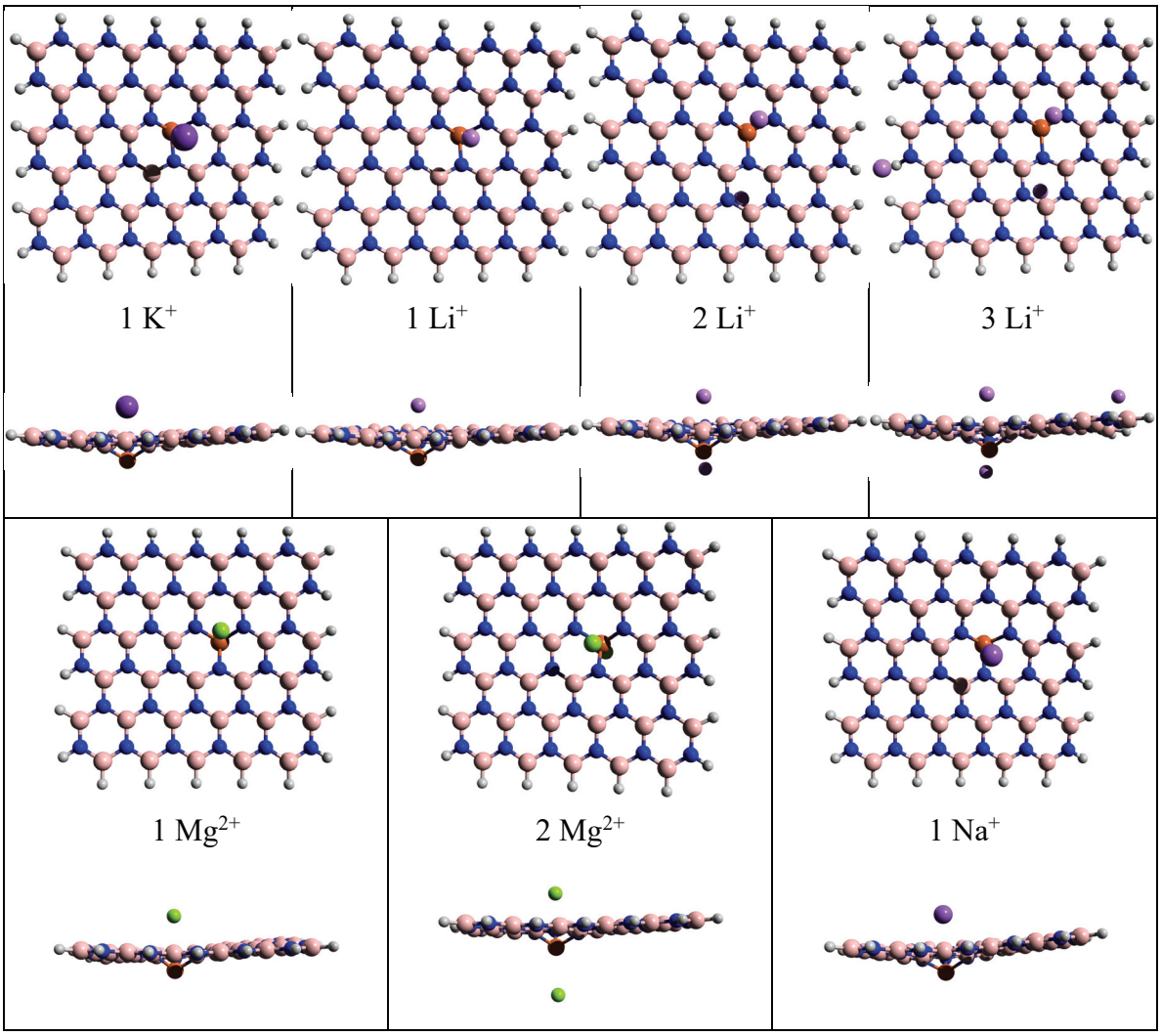

Figure 3.22. Optimized structure of ion loaded top and side view of Fe-doped BNN

Table 3.6. Adsorption energy (E_{ads}), voltage of the corresponding negative electrode material (V_{cell}), theoretical specific capacity (C_c) and theoretical volume change between the charged and discharged states (ΔV) for 100 g of material of Fe-doped BNN

Name	E_{ads} (kcal/mol)	V_{cell} (V)	C_c(mAh/g)	ΔV (cm^3)
Fe-BNN + K^+	-38.43	1.29	57.88	2.76
Fe-BNN + Li^+	-56.87	2.03	62.20	5.38
Fe-BNN + $2Li^+$	-45.11	1.14	122.42	7.10
Fe-BNN + $3Li^+$	-4.31	-1.01	180.77	11.89
Fe-BNN + Mg^{2+}	-194.34	8.09	119.57	-1.78
Fe-BNN + $2Mg^{2+}$	-155.33	6.19	226.85	11.02
Fe-BNN + Na^+	-50.00	1.75	59.96	4.69

For the Ga-doped BNN structure, the maximum ion holding capacity is 2 for K, Li, and Na, while it is 1 for Mg (see Figure 3.23). All cases are thermodynamically favorable. For potassium batteries, the cell voltage is within the desired range of 0.16-0.85 V (see Table 3.7). The maximum theoretical specific capacity found is 103.87 mAh/g, and the change in volume when the battery is full is quite low at 4.71 cm^3. For lithium batteries, this material has a relatively high voltage, ranging between 1.16 and 1.44 volts. Its maximum specific capacity is 118.66 mAh/g, but the change in volume when holding two ions is quite high, with about 34 cm^3 of volume expansion for 100 grams of material. A similar situation applies to magnesium ions. Even though it can hold only one magnesium ion, there is about 20 cm^3 of expansion in volume. However, despite the high theoretical capacity, the voltage value is quite high. Results for sodium-ion batteries are similar to potassium. The specific capacity can go up to 110.79 mAh/g, while the change in volume remains at 4.76 cm^3. The voltage value stays below 2 V as desired.

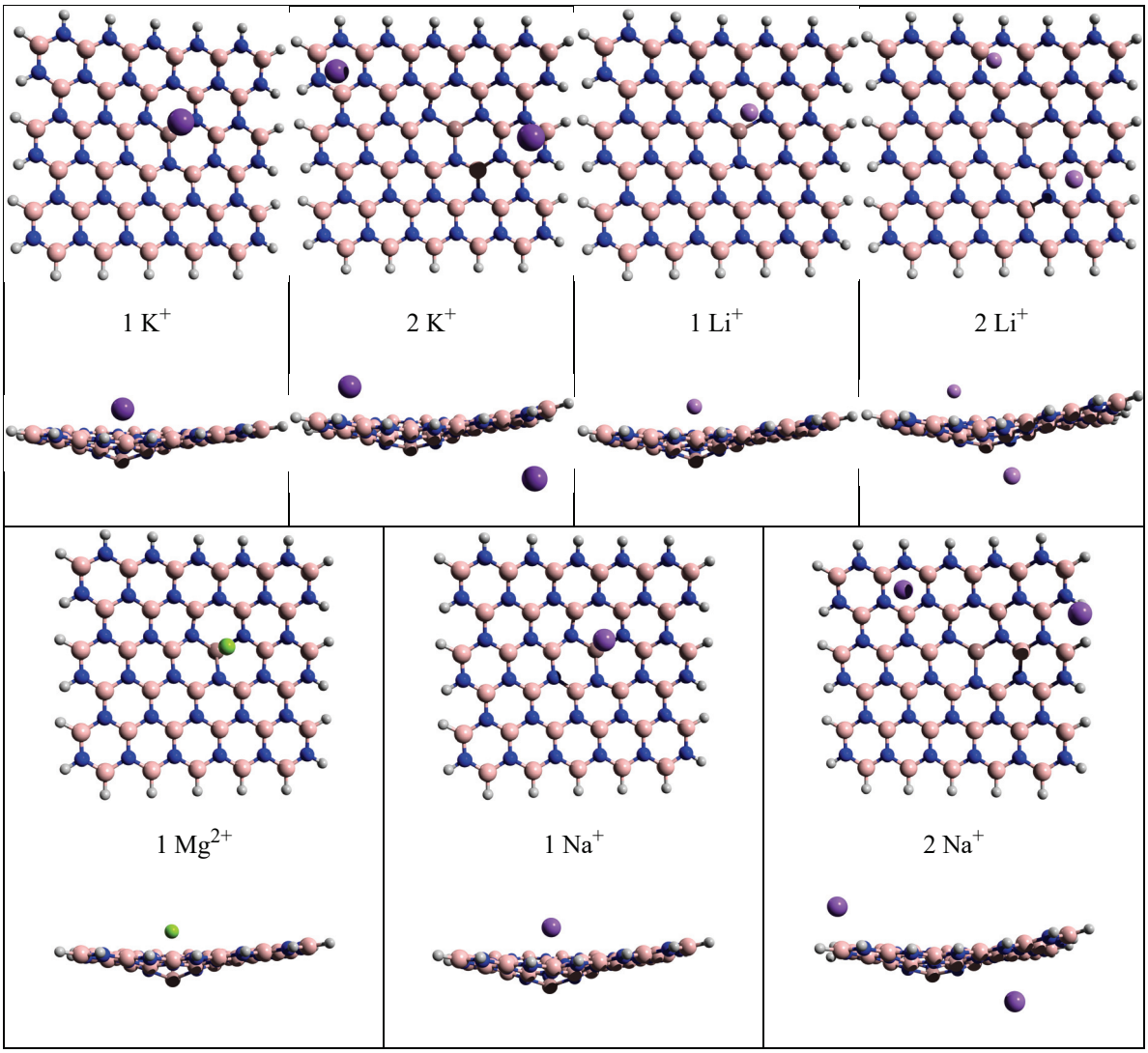

Figure 3.23. Optimized structure of ion loaded top and side view of Ga-doped BNN

Table 3.7. Adsorption energy (E_{ads}), voltage of the corresponding negative electrode material (V_{cell}), theoretical specific capacity (C_c) and theoretical volume change between the charged and discharged states (ΔV) for 100 g of material of Fe-doped BNN

Name	E_{ads} (kcal/mol)	V_{cell} (V)	C_c(mAh/g)	ΔV (cm^3)
Ga-BNN + K^+	-27.94	0.85	56.19	8.43
Ga-BNN + $2K^+$	-21.03	0.16	103.87	4.71
Ga-BNN + Li^+	-42.43	1.44	60.26	8.72
Ga-BNN + $2Li^+$	-40.83	1.16	118.66	34.01
Ga-BNN + Mg^{2+}	-172.14	7.11	115.98	20.08
Ga-BNN + Na^+	-38.65	1.29	58.16	7.87
Ga-BNN + $2Na^+$	-35.33	0.73	110.79	4.76

Unlike other BNN surfaces, the O-doped BNN structure could be optimized with 3 sodium ions, but again in the structure with 3 ions, the binding energies of the ions with the surface are not favorable (see Figure 3.24). Therefore, we need to examine the structure with 2 sodium ions. The maximum theoretical capacity can reach up to 124.63 mAh/g, while the change in volume is only 8.72 cm^3 (see Table 3.8). Looking at the voltage, being in the range of 1.06 to 1.83 V also shows that O-doped BNN is a suitable anode material for sodium under these conditions. Similar results were obtained for potassium and lithium batteries. The maximum theoretical specific capacity for the potassium-ion battery is 115.94 mAh/g, while for the lithium-ion battery, it was found to be 134.68 mAh/g. The change in the Van der Waals volume of the surface is at most 10.82 cm^3. For potassium and lithium-ion batteries, the voltage value is high for lithium but within a suitable range for potassium (0.64 – 1.40 V). When we come to magnesium, the formation of covalent bonds between it and the nitrogens was observed again. The high voltage value (10.18 V) and adsorption energy (244.61 kcal/mol) confirm this. Moreover, the change in the Van der Waals volume is also high at 19.62 cm^3.

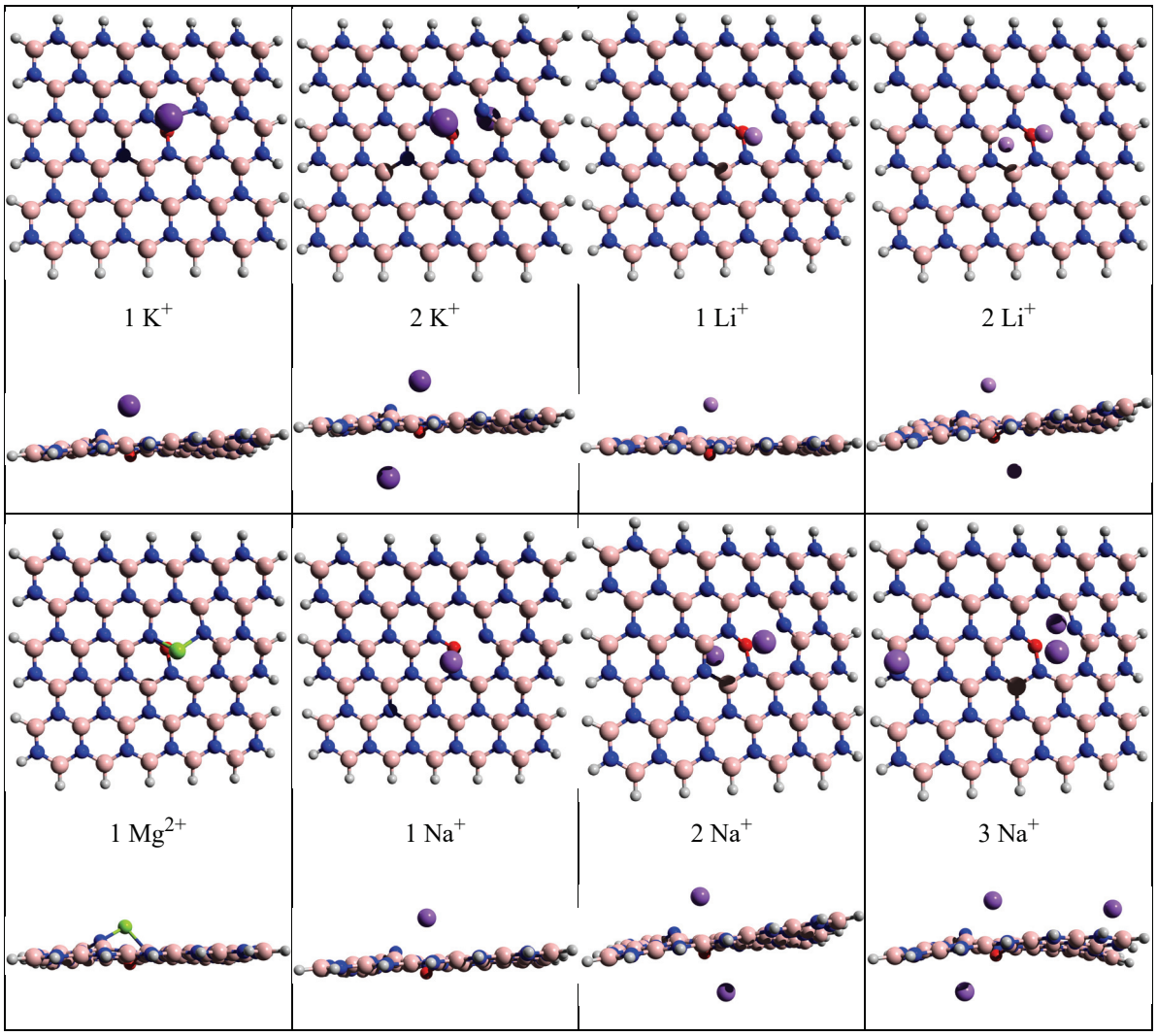

Figure 3.24. Optimized structure of ion loaded top and side view of O-doped BNN

Table 3.8. Adsorption energy (E_{ads}), voltage of the corresponding negative electrode material (V_{cell}), theoretical specific capacity (C_c) and theoretical volume change between the charged and discharged states (ΔV) for 100 g of material of O-doped BNN

Name	E_{ads} (kcal/mol)	V_{cell} (V)	C_c(mAh/g)	ΔV (cm^3)
O-BNN + K^+	-41.01	1.40	63.33	4.10
O-BNN + $2K^+$	-31.03	0.64	115.94	7.20
O-BNN + Li^+	-60.68	2.20	68.53	4.27
O-BNN + $2Li^+$	-52.48	1.52	134.68	10.82
O-BNN + Mg^{2+}	-244.61	10.18	131.24	19.62
O-BNN + Na^+	-51.71	1.83	65.83	3.36
O-BNN + $2Na^+$	-41.54	1.06	124.63	8.72
O-BNN + $3Na^+$	2.28	-1.23	177.45	13.35

The results showed that the P-doped BNN structure is suitable for anode material usage in potassium, lithium, and sodium ion batteries. However, the energy capacities did not surpass those of commercial lithium batteries. The maximum energy capacities for potassium, lithium, and sodium ion batteries were found to be 112.30 mAh/g, 129.79 mAh/g, and 120.43 mAh/g, respectively for the P-doped BNN. When looking at the change in the Van der Waals volume for 100 grams of material, no significant change is observed among these ions, which is desired. The maximum number of ions that can be stored for the lithium battery was found to be 3, and this structure could be optimized. Although the adsorption energy has a negative value, the voltage value of -0.99 theoretically indicates that the battery would not work in practice in this manner. When magnesium ions were loaded into the system, the formation of a covalent bond was observed again. Similar to the Co-doped BNN structure, the magnesium ion displaces the dopant and positions itself closer to the surface at a shorter distance than the dopant. The high voltage value confirms this situation while causing a significant change in the Van der Waals volume.

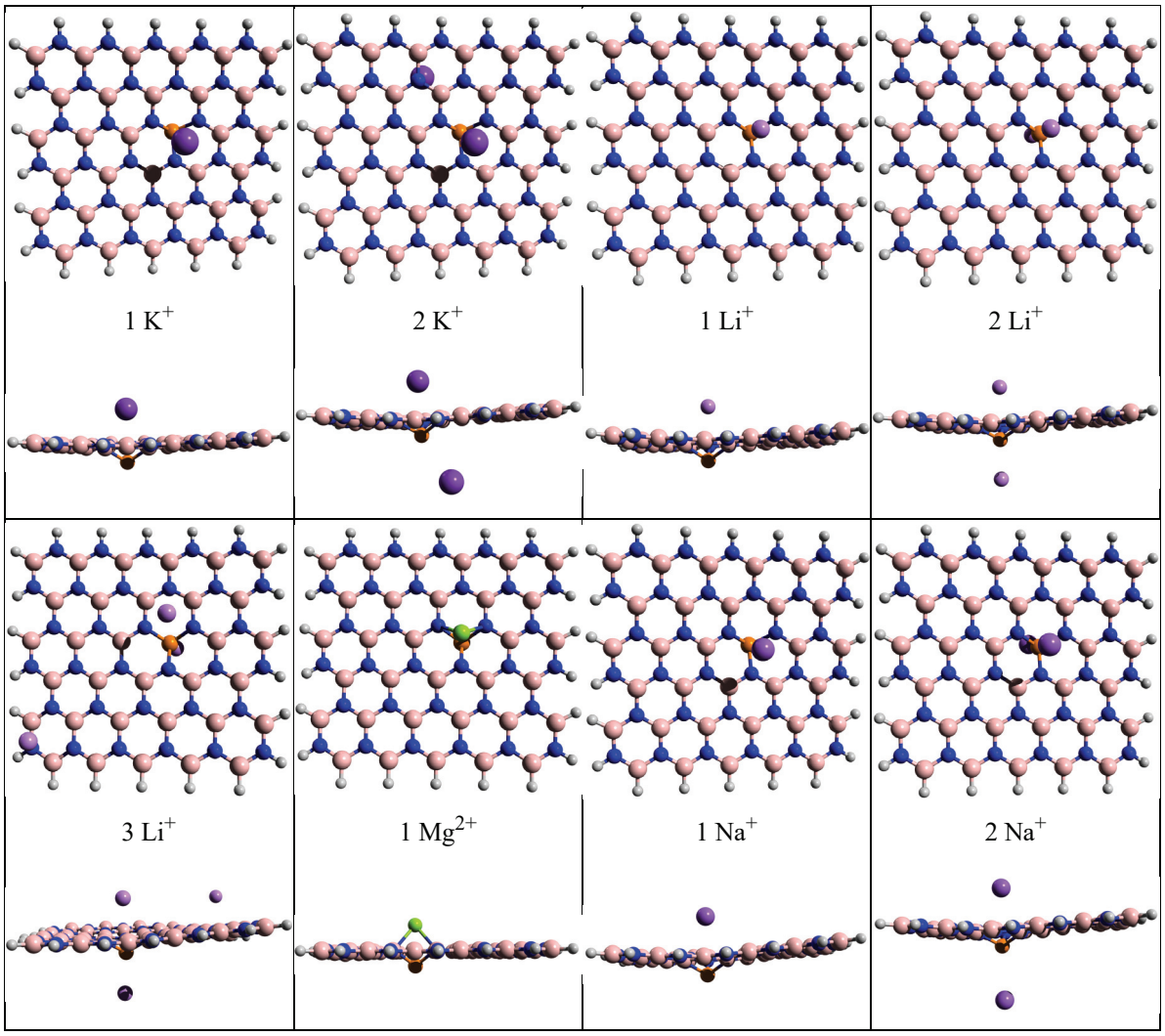

Figure 3.25. Optimized structure of ion loaded top and side view of P-doped BNN

Table 3.9. Adsorption energy (E_{ads}), voltage of the corresponding negative electrode material (V_{cell}), theoretical specific capacity (C_c) and theoretical volume change between the charged and discharged states (ΔV) for 100 g of material of P-doped BNN

Name	E_{ads} (kcal/mol)	V_{cell} (V)	C_c(mAh/g)	ΔV (cm^3)
P-BNN + K^+	-35.82	1.17	61.16	3.85
P-BNN + $2K^+$	-23.67	0.28	112.30	4.79
P-BNN + Li^+	-53.15	1.89	66.01	4.49
P-BNN + $2Li^+$	-44.67	1.25	129.79	2.09
P-BNN + $3Li^+$	-2.33	-0.99	191.47	7.42
P-BNN + Mg^{2+}	-224.58	9.29	126.60	15.56
P-BNN + Na^+	-46.82	1.63	63.50	3.60
P-BNN + $2Na^+$	-33.11	0.76	120.43	1.38

According to DFT results, the likelihood of the S-doped BNN structure serving as an anode material for potassium and magnesium ion batteries is low. When the second ion was added to these batteries, the ions did not remain stable on the surface. A theoretical specific capacity of 61.01 mAh/g was calculated for potassium, while for magnesium, it was determined as 126.27 mAh/g. In this example, despite high adsorption and high voltage for the magnesium battery, no covalent bond formation was observed. This indicates a strong attachment of the sulfur dopant to the structure. In fact, with the introduction of the magnesium ion, the Van der Waals volume in 100 grams of material was calculated to decrease by 15.77 cm^3. When examining the capacity of this structure to serve as an anode material for the lithium-ion battery, it was shown to have favorable adsorption (-49.53 kcal/mol) and cell voltage (1.42 V) values for 2 lithium ions. For the sodium-ion battery, these values were -39.86 kcal/mol, while the voltage value was 0.94 V. For both ions, the maximum theoretical specific capacity of this structure was found to be around 120-130 mAh/g. The changes in the Van der Waals volume in charged-discharged states for 100 grams of material were advantageously low, at approximately 6 cm^3.

The ion capacities and their nearest distances from the doped surfaces are presented in Table 3.10, for the ions investigated in this study. Generally, the distances from the surface to the ions tend to increase with the cationic size of the ions, with the exception of Fe-doped and S-doped surfaces. For most anode surfaces, the maximum ion capacity for the type of ion battery studied is found to be 2, except for Fe doped with Na and K ions, and S doped with K ion. The nearest distances from the surfaces range between 2.6 Å to 2.9 Å for Li ions, 2.9 Å to 3.3 Å for Na ions, and 2.7 Å to 3.8 Å for K ions.

Table 3.10. Ion capacities and their nearest distances (Å) from the doped surfaces.

Dopants	Ion capacity R(Li-surface)	Ion capacity R(Na-surface)	Ion capacity R(K-surface)
Al	2 2.82	2 3.14	2 3.74
Co	2 2.8	2 3.29	2 3.76
Fe	2 2.85	1 3.2	1 2.89
Ga	2 2.81	2 3.06	2 3.3
O	2 2.61	2 2.93	2 3.18
P	2 2.7	2 3.29	2 3.34
S	2 2.66	2 3.08	1 2.7

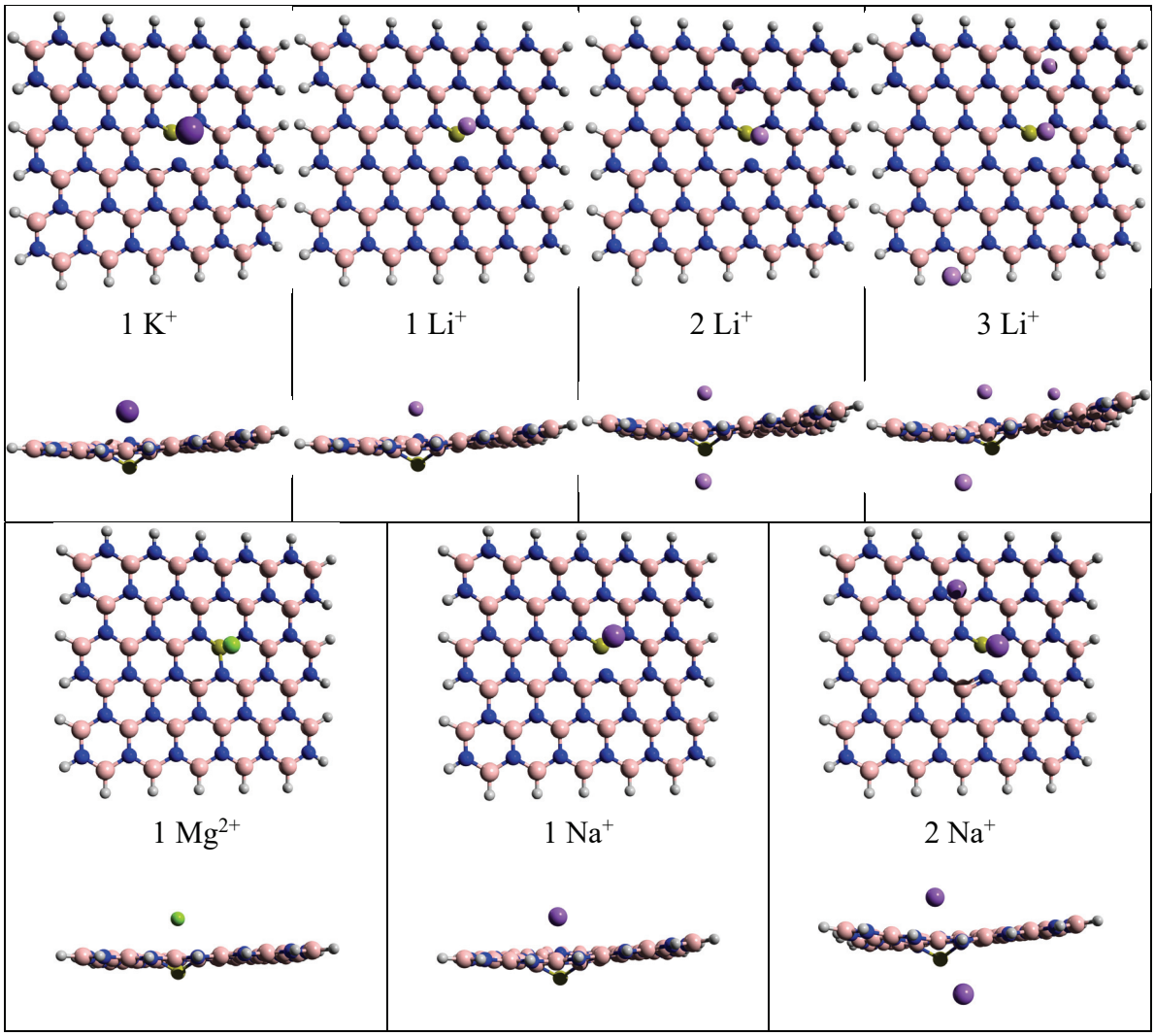

Figure 3.26. Optimized structure of ion loaded top and side view of S-doped BNN

Table 3.11. Adsorption energy (E_{ads}), voltage of the corresponding negative electrode material (V_{cell}), theoretical specific capacity (C_c) and theoretical volume change between the charged and discharged states (ΔV) for 100 g of material of S-doped BNN

Name	E_{ads} (kcal/mol)	V_{cell} (V)	C_c(mAh/g)	ΔV (cm^3)
S-BNN + K^+	-40.39	1.36	61.01	4.67
S-BNN + Li^+	-60.07	2.18	65.83	6.15
S-BNN + $2Li^+$	-49.53	1.42	129.45	8.67
S-BNN + 3Li+	-10.24	-0.66	190.98	13.42
S-BNN + Mg^{2+}	-242.37	10.11	126.27	-15.77
S-BNN + Na^+	-51.69	1.83	63.33	4.87
S-BNN + 2Na+	-39.86	0.94	120.14	6.45

CHAPTER 4

CONCLUSION

In this thesis, the doping effect on the electronic and structural properties of 2D BNN material have been investigated by quantum chemical calculations at the B3LYP/def2-SVP/D4/gCP level of theory. The dopants which are Al, Cl, Co, Fe, Ga, O, P, S atoms are used to address whether the doped BNN have the potential to be an anode material for the K, Li, Mg, Na ion batteries.

The conductivities are discussed through the energy gap of HOMO and LUMO orbitals. Semi-empirical tight binding combined with meta-dynamics methods and density functional theory were utilized to discover these properties.

The conductivity of pristine BNN affected significantly by the Co, Fe and S doping of BNN structure. The increase in conductivity is found as 35%, 34% and 26% for Co, Fe and S respectively. The HOMO and LUMO structures showed that, Al and Ga doped BNN have similar HOMO electron density, these dopants act as an electron acceptor, the net charge transfer was observed from nitrogen atoms upon HOMO to LUMO transition. On the contrary, O, S and P atoms donated their electrons to boron atoms of corresponding doped BNN, they have almost the same electron density on LUMO.

The BNN surface tilted by the doping Ga and Al atoms. The other dopants have not affected much the overall surface structure, but cause a local change. Cl atom stayed on the planar BNN surface while the other dopant atoms located a little far from the BNN.

The goal was to achieve structures with high theoretical specific capacity, low anode electrode voltage, and minimal volume change between charged/discharged states. It was observed that none of the studied BNN structures favorable for the use in magnesium ion batteries. Although magnesium's 2+ charge might suggest a higher theoretical capacity, the strong interactions caused by the high charge and resulting high voltage led to poor performance in the anode materials usage of it. Although potassium batteries showed similar performance to lithium and sodium batteries, their heavier weight per gram meant that the theoretical specific capacity could not compete with lithium and sodium. Most of the doped BNN within this work could be used as anode

materials according to these results. However, none of them possess a better capacity than classic lithium batteries.

Considering the ideal scenario for the suggested BNN structures to serve as anode materials, the best results for Al-doped BNN were seen in its suitability for lithium-ion batteries. Cl-doped BNN was found unsuitable as anode for any K, Li, Mg, and Na batteries due to high voltage. Co-doped BNN showed the best results in lithium-ion batteries. Fe-doped BNN performed best in lithium-ion batteries. The best results for Ga-doped BNN were found in sodium-ion batteries. O-doped BNN, P-doped BNN, and S-doped BNN showed the best performance in lithium-ion batteries and then in sodium-ion batteries. Among all structures, the O-doped BNN structure exhibited the highest performance with an energy density of 134.68 mAh/g.

For the sake of the computation time and resources, 2D-BNN monolayer model was chosen in our calculations, we did not account the periodicity. If the periodic boundary condition was included, we believe better energy densities could be obtained.

REFERENCES

Ahmed, Tanvir, Md. Aminur Rahman, Rafiqul Islam, Afiya Akter Piya, and Siraj Ud Daula Shamim. 2022. "Unravelling the Adsorption Performance of BN, AlN, GaN and InN 2D Nanosheets towards the Ciclopirox, 5-Fluorouracil and Nitrosourea for Anticancer Drug Delivery Motive: A DFT-D with QTAIM, PCM and COSMO Investigations." *Computational and Theoretical Chemistry* 1214 (August): 113797. https://doi.org/10.1016/j.comptc.2022.113797.

Amorim, Rodrigo G, Xiaoliang Zhong, Saikat Mukhopadhyay, Ravindra Pandey, Alexandre R Rocha, and Shashi P Karna. 2013. "Strain- and Electric Field-Induced Band Gap Modulation in Nitride Nanomembranes." *Journal of Physics: Condensed Matter* 25 (19): 195801. https://doi.org/10.1088/0953-8984/25/19/195801.

Anthony King. 2023. "Northvolt to Bring Sodium-Ion Batteries to European Market." *Chemistry World*, November 23, 2023.

Bannwarth, Christoph, Sebastian Ehlert, and Stefan Grimme. 2019. "GFN2-XTB—An Accurate and Broadly Parametrized Self-Consistent Tight-Binding Quantum Chemical Method with Multipole Electrostatics and Density-Dependent Dispersion Contributions." *Journal of Chemical Theory and Computation* 15 (3): 1652–71. https://doi.org/10.1021/acs.jctc.8b01176.

Becke, Axel D. 1993. "Density-Functional Thermochemistry. III. The Role of Exact Exchange." *The Journal of Chemical Physics* 98 (7): 5648–52. https://doi.org/10.1063/1.464913.

Bhauriyal, Preeti, Arup Mahata, and Biswarup Pathak. 2018. "Graphene-like Carbon–Nitride Monolayer: A Potential Anode Material for Na- and K-Ion Batteries." *The Journal of Physical Chemistry C* 122 (5): 2481–89. https://doi.org/10.1021/acs.jpcc.7b09433.

Caldeweyher, Eike, Sebastian Ehlert, Andreas Hansen, Hagen Neugebauer, Sebastian Spicher, Christoph Bannwarth, and Stefan Grimme. 2019. "A Generally Applicable Atomic-Charge Dependent London Dispersion Correction." *The Journal of Chemical Physics* 150 (15). https://doi.org/10.1063/1.5090222.

Chakrabarti, Shamik, Arvind Singh, and A.K. Thakur. 2023. "Density Functional Theory Study of SnSe2 as Anode Material for Mg Ion Battery Application." *Computational Condensed Matter* 35 (June): e00800. https://doi.org/10.1016/j.cocom.2023.e00800.

Chombo, Pius Victor, and Yossapong Laoonual. 2020. "A Review of Safety Strategies of a Li-Ion Battery." *Journal of Power Sources* 478 (December): 228649. https://doi.org/10.1016/J.JPOWSOUR.2020.228649.

Das, Sudipto, Siraj Ud Daula Shamim, Md. Kamal Hossain, Farid Ahmed, Md. Abul Hossain, and Mohammad Obaidur Rahman. 2022. "A Novel Silicon-Doped 2D Ti2C MXene Monolayer as High Capacity Stable Anode Material for Lithium Ion Batteries: Insight from Density Functional Theory Study." *Applied Surface Science* 600 (October): 154173. https://doi.org/10.1016/j.apsusc.2022.154173.

Duhan, Nidhi, and T. J. Dhilip Kumar. 2024. "Ab Initio Study of Li-Shrouded Si-Doped γ-Graphyne Nanosheet as Propitious Anode in Li-Ion Batteries." *Applied Surface Science* 642 (January): 158553. https://doi.org/10.1016/J.APSUSC.2023.158553.

Ghosh, Sourav, Maxim A. Makeev, Martina Lucia Macaggi, Zhimin Qi, Haiyan Wang, Nav Nidhi Rajput, Surendra K. Martha, and Vilas G. Pol. 2020. "Dipotassium Terephthalate as Promising Potassium Storing Anode with DFT Calculations." *Materials Today Energy* 17 (September): 100454. https://doi.org/10.1016/j.mtener.2020.100454.

Goikolea, Eider, Verónica Palomares, Shijian Wang, Idoia Ruiz de Larramendi, Xin Guo, Guoxiu Wang, and Teofilo Rojo. 2020. "Na-Ion Batteries—Approaching Old and New Challenges." *Advanced Energy Materials* 10 (44). https://doi.org/10.1002/aenm.202002055.

Gu, Mubao, Junling Xu, Xiaoyan Shi, Lianyi Shao, and Zhipeng Sun. 2024. "Research Progress of Oxygen Redox in Sodium-layered Oxides." *Battery Energy*, January. https://doi.org/10.1002/bte2.20230046.

Guo, Qi, Wen Zeng, Shi-Lin Liu, Yan-Qiong Li, Jun-Yao Xu, Jin-Xing Wang, and Yu Wang. 2021. "Recent Developments on Anode Materials for Magnesium-Ion Batteries: A Review." *Rare Metals* 40 (2): 290–308. https://doi.org/10.1007/s12598-020-01493-3.

Guo, Yong-sheng, Fan Zhang, Jun Yang, Fei-fei Wang, Yanna NuLi, and Shin-ichi Hirano. 2012. "Boron-Based Electrolyte Solutions with Wide Electrochemical Windows for Rechargeable Magnesium Batteries." *Energy & Environmental Science* 5 (10): 9100. https://doi.org/10.1039/c2ee22509c.

Hanwell, Marcus D, Donald E Curtis, David C Lonie, Tim Vandermeersch, Eva Zurek, and Geoffrey R Hutchison. 2012. "Avogadro: An Advanced Semantic Chemical Editor, Visualization, and Analysis Platform." *Journal of Cheminformatics* 4 (1): 17. https://doi.org/10.1186/1758-2946-4-17.

Hod, Oded. 2012. "Graphite and Hexagonal Boron-Nitride Have the Same Interlayer Distance. Why?" *Journal of Chemical Theory and Computation* 8 (4): 1360–69. https://doi.org/10.1021/ct200880m.

Hohenberg, P., and W. Kohn. 1964. "Inhomogeneous Electron Gas." *Physical Review* 136 (3B): B864–71. https://doi.org/10.1103/PhysRev.136.B864.

Hosseinian, A., S. Soleimani-amiri, S. Arshadi, E. Vessally, and L. Edjlali. 2017. "Boosting the Adsorption Performance of BN Nanosheet as an Anode of Na-Ion Batteries: DFT Studies." *Physics Letters A* 381 (24): 2010–15. https://doi.org/10.1016/j.physleta.2017.04.022.

Huang, Yanghang, Haochen Yang, Yi Zhang, Yamin Zhang, Yutong Wu, Mengkun Tian, Peng Chen, et al. 2019. "A Safe and Fast-Charging Lithium-Ion Battery Anode Using MXene Supported Li3VO4." *Journal of Materials Chemistry A* 7 (18): 11250–56. https://doi.org/10.1039/C9TA02037C.

Hueso, Karina B., Michel Armand, and Teófilo Rojo. 2013. "High Temperature Sodium Batteries: Status, Challenges and Future Trends." *Energy & Environmental Science* 6 (3): 734. https://doi.org/10.1039/c3ee24086j.

Hussain, Tanveer, Hakkim Vovusha, Thanayut Kaewmaraya, Vittaya Amornkitbamrung, and Rajeev Ahuja. 2018. "Adsorption Characteristics of DNA Nucleobases, Aromatic Amino Acids and Heterocyclic Molecules on Silicene and Germanene Monolayers." *Sensors and Actuators B: Chemical* 255 (February): 2713–20. https://doi.org/10.1016/j.snb.2017.09.083.

Jian, Zelang, Yong Chen, Fujun Li, Tao Zhang, Chang Liu, and Haoshen Zhou. 2014. "High Capacity Na–O2 Batteries with Carbon Nanotube Paper as Binder-Free Air Cathode." *Journal of Power Sources* 251 (April): 466–69. https://doi.org/10.1016/j.jpowsour.2013.11.091.

Jin, Chuanhong, Fang Lin, Kazu Suenaga, and Sumio Iijima. 2009. "Fabrication of a Freestanding Boron Nitride Single Layer and Its Defect Assignments." *Physical Review Letters* 102 (19): 195505. https://doi.org/10.1103/PhysRevLett.102.195505.

Kadhim, Mustafa M., Taleeb Zedan Taban, Sallal A.H. Abdullaha, Ahmed Mahdi Rheima, Safa K. Hachim, and Azher M. Abed. 2023. "Potential Use of Silicon Carbide Monolayer as an Anode in Rechargeable Mg-Ion Batteries." *Journal of Physics and Chemistry of Solids* 177 (June): 111270. https://doi.org/10.1016/j.jpcs.2023.111270.

Kang, Jungmin, Jinho Ahn, Yongseok Lee, Hyunyoung Park, Wonseok Ko, Bonyoung Ku, Myungeun Choi, Hun-Gi Jung, Won-Hee Ryu, and Jongsoon Kim. 2023. "Chiolite Na5Ti3F14: A Novel Sodium Titanium Fluoride Anode for Low-Cost and High-Performance Na-Ion Batteries." *Energy Storage Materials* 63 (November): 103048. https://doi.org/10.1016/j.ensm.2023.103048.

Khan, Adnan Ali, Rashid Ahmad, and Iftikhar Ahmad. 2021. "Silicon Carbide and III-Nitrides Nanosheets: Promising Anodes for Mg-Ion Batteries." *Materials Chemistry and Physics* 257 (January): 123785. https://doi.org/10.1016/j.matchemphys.2020.123785.

Kohn, W., and L. J. Sham. 1965. "Quantum Density Oscillations in an Inhomogeneous Electron Gas." *Physical Review* 137 (6A): A1697–1705. https://doi.org/10.1103/PhysRev.137.A1697.

Kruse, Holger, and Stefan Grimme. 2012. "A Geometrical Correction for the Inter- and Intra-Molecular Basis Set Superposition Error in Hartree-Fock and Density Functional Theory Calculations for Large Systems." *The Journal of Chemical Physics* 136 (15). https://doi.org/10.1063/1.3700154.

Kubota, Kei, and Shinichi Komaba. 2015. “Review—Practical Issues and Future Perspective for Na-Ion Batteries.” *Journal of The Electrochemical Society* 162 (14): A2538–50. https://doi.org/10.1149/2.0151514jes.

Lakshmy, Seetha, Gopal Sanyal, Nandakumar Kalarikkal, and Brahmananda Chakraborty. 2023. “Pristine and Metal Decorated Biphenylene Monolayer for Enhanced Adsorption of Nitrobenzene: A DFT Approach.” *Applied Surface Science* 613 (March): 155995. https://doi.org/10.1016/j.apsusc.2022.155995.

Landi, Brian J., Matthew J. Ganter, Cory D. Cress, Roberta A. DiLeo, and Ryne P. Raffaelle. 2009. “Carbon Nanotubes for Lithium Ion Batteries.” *Energy & Environmental Science* 2 (6): 638. https://doi.org/10.1039/b904116h.

Li, Chunyue, Yuanhua Lin, Xing Li, Zhonghui Li, Pan Luo, Yifu Jin, and Zishuo Li. 2023. “Effect of Co-Doping Concentration on α-Fe2O3/Graphene as Anode Materials for Lithium Ion Batteries.” *Colloids and Surfaces A: Physicochemical and Engineering Aspects* 660 (March): 130681. https://doi.org/10.1016/j.colsurfa.2022.130681.

Li, Liuying, Yaxing Ren, Kieran O’Regan, Upender Rao Koleti, Emma Kendrick, W. Dhammika Widanage, and James Marco. 2021. “Lithium-Ion Battery Cathode and Anode Potential Observer Based on Reduced-Order Electrochemical Single Particle Model.” *Journal of Energy Storage* 44 (December): 103324. https://doi.org/10.1016/J.EST.2021.103324.

Li, Matthew, Jun Lu, Zhongwei Chen, and Khalil Amine. 2018. “30 Years of Lithium-Ion Batteries.” *Advanced Materials* 30 (33): 1800561. https://doi.org/10.1002/ADMA.201800561.

Liu, Hanlin, Wang Yang, Sai Che, Yun Li, Cong Xu, Xin Wang, Guang Ma, Guoyong Huang, and Yongfeng Li. 2022. “Silicon Doped Graphene as High Cycle Performance Anode for Lithium-Ion Batteries.” *Carbon* 196 (August): 633–38. https://doi.org/10.1016/j.carbon.2022.05.018.

Liu, Lu, Xiaopeng Guan, Hongjia Song, Yong Tang, Xiangli Zhong, Jinbin Wang, Daifeng Zou, and Juanjuan Cheng. 2023. “Effects of Si, B Doping on PC3 Monolayer as Anode for Na-Ion Batteries.” *Physica E: Low-Dimensional Systems*

and Nanostructures 152 (August): 115742. https://doi.org/10.1016/j.physe.2023.115742.

Liu, Shude, Ling Kang, Joel Henzie, Jian Zhang, Jisang Ha, Mohammed A. Amin, Md Shahriar A. Hossain, Seong Chan Jun, and Yusuke Yamauchi. 2021. "Recent Advances and Perspectives of Battery-Type Anode Materials for Potassium Ion Storage." *ACS Nano* 15 (12): 18931–73. https://doi.org/10.1021/acsnano.1c08428.

Liu, Wen, Qian Sun, Yin Yang, Jing-Ying Xie, and Zheng-Wen Fu. 2013. "An Enhanced Electrochemical Performance of a Sodium–Air Battery with Graphene Nanosheets as Air Electrode Catalysts." *Chemical Communications* 49 (19): 1951. https://doi.org/10.1039/c3cc00085k.

Liu, Yujie, Ming Ren, Bo Song, and Ming Dong. 2023. "A DFT Study of Toxic Gases (NH3, C2H2, NO) Adsorption and Detection on Metal Oxides (CuO, Ag2O, In2O3) Modified MoTe2 Monolayer." *Applied Surface Science* 622 (June): 156858. https://doi.org/10.1016/j.apsusc.2023.156858.

Lu, Z., A. Schechter, M. Moshkovich, and D. Aurbach. 1999. "On the Electrochemical Behavior of Magnesium Electrodes in Polar Aprotic Electrolyte Solutions." *Journal of Electroanalytical Chemistry* 466 (2): 203–17. https://doi.org/10.1016/S0022-0728(99)00146-1.

Maglic, Jasmin B., and Roy Lavendomme. 2022. "*MoloVol* : An Easy-to-Use Program for Analyzing Cavities, Volumes and Surface Areas of Chemical Structures." *Journal of Applied Crystallography* 55 (4): 1033–44. https://doi.org/10.1107/S1600576722004988.

Massé, Robert C., Evan Uchaker, and Guozhong Cao. 2015. "Beyond Li-Ion: Electrode Materials for Sodium- and Magnesium-Ion Batteries." *Science China Materials* 58 (9): 715–66. https://doi.org/10.1007/s40843-015-0084-8.

Mei, Tiantian, Jianbao Wu, Shuhan Lu, Bingqian Wang, Xinxin Zhao, Lili Wang, and Zhixiang Yin. 2021. "A DFT Study on AlN Nanotubes and Nanosheets as Anodes for Mg-Ion Batteries." *Computational and Theoretical Chemistry* 1203 (September): 113352. https://doi.org/10.1016/j.comptc.2021.113352.

Nazneen, Farzana, Prianka Mondal, Naafis Ahnaf Shahed, Shamima Khanom, Md. Kamal Hossain, and Farid Ahmed. 2023. "T-BN Nanosheets as High-Capacity Anode for Li- and Na-Ion Batteries: An Ab Initio Study." *Computational and Theoretical Chemistry* 1224 (June): 114105. https://doi.org/10.1016/j.comptc.2023.114105.

Neese, Frank. 2012. "The ORCA Program System." *WIREs Computational Molecular Science* 2 (1): 73–78. https://doi.org/10.1002/wcms.81.

Nejati, K., A. Hosseinian, A. Bekhradnia, E. Vessally, and L. Edjlali. 2017. "Na-Ion Batteries Based on the Inorganic BN Nanocluster Anodes: DFT Studies." *Journal of Molecular Graphics and Modelling* 74 (June): 1–7. https://doi.org/10.1016/j.jmgm.2017.03.001.

Nelson, Emily G., Scott I. Brody, Jeff W. Kampf, and Bart M. Bartlett. 2014. "A Magnesium Tetraphenylaluminate Battery Electrolyte Exhibits a Wide Electrochemical Potential Window and Reduces Stainless Steel Corrosion." *J. Mater. Chem. A* 2 (43): 18194–98. https://doi.org/10.1039/C4TA04625K.

Newman, Gerald H., and Lawrence P. Klemann. 1980. "Ambient Temperature Cycling of an Na - TiS2 Cell." *Journal of The Electrochemical Society* 127 (10): 2097–99. https://doi.org/10.1149/1.2129353.

Nitta, Naoki, Feixiang Wu, Jung Tae Lee, and Gleb Yushin. 2015. "Li-Ion Battery Materials: Present and Future." *Materials Today* 18 (5): 252–64. https://doi.org/10.1016/J.MATTOD.2014.10.040.

Orio, Maylis, Dimitrios A. Pantazis, and Frank Neese. 2009. "Density Functional Theory." *Photosynthesis Research* 102 (2–3): 443–53. https://doi.org/10.1007/s11120-009-9404-8.

Oshima, Taku, Masaharu Kajita, and Akiyasu Okuno. 2004. "Development of Sodium-Sulfur Batteries." *International Journal of Applied Ceramic Technology* 1 (3): 269–76. https://doi.org/10.1111/j.1744-7402.2004.tb00179.x.

Peled, E., C. Menachem, D. Bar-Tow, and A. Melman. 1996. "Improved Graphite Anode for Lithium-Ion Batteries Chemically: Bonded Solid Electrolyte Interface and

Nanochannel Formation." *Journal of The Electrochemical Society* 143 (1): L4–7. https://doi.org/10.1149/1.1836372/XML.

Pereira, Florbela, Kaixia Xiao, Diogo A. R. S. Latino, Chengcheng Wu, Qingyou Zhang, and Joao Aires-de-Sousa. 2017. "Machine Learning Methods to Predict Density Functional Theory B3LYP Energies of HOMO and LUMO Orbitals." *Journal of Chemical Information and Modeling* 57 (1): 11–21. https://doi.org/10.1021/acs.jcim.6b00340.

Pracht, Philipp, Fabian Bohle, and Stefan Grimme. 2020. "Automated Exploration of the Low-Energy Chemical Space with Fast Quantum Chemical Methods." *Physical Chemistry Chemical Physics* 22 (14): 7169–92. https://doi.org/10.1039/C9CP06869D.

Rajhi, Ali A., Eduardo Hernández, Carlos Serrano, Shelesh Krishna Saraswat, Ahmed Mohammed Mahmood, Hayder sharif, Y.A. Abdulsayed, and Ahmed Alawadi. 2023. "Exploring the Potential of Di-Boron Di-Nitride Monolayer (o-B2N2) as a K-Ion Battery Anode: A DFT Study." *Physica B: Condensed Matter* 669 (November): 415324. https://doi.org/10.1016/j.physb.2023.415324.

Riyaz, Mohd, Shivangi Garg, Navjot Kaur, and Neetu Goel. 2022. "Boron Doped Graphene as Anode Material for Mg Ion Battery: A DFT Study." *Computational and Theoretical Chemistry* 1214 (August): 113757. https://doi.org/10.1016/j.comptc.2022.113757.

Saadh, Mohamed J., Victor Bravo, Ember Geovanny Zumba Novay, Anjan Kumar, Sanaa Fathy Mahmud, Noor Abd Alkhudhur Salman, Nerain Mohammed, Luis Buenaño, and Yasser Elmasry. 2024. "A DFT Study on the Application of B, N, and BN-Doped Phagraphene in Na-Ion Batteries." *Diamond and Related Materials* 141 (January): 110645. https://doi.org/10.1016/j.diamond.2023.110645.

Saritha, D., and R. Sujithra. 2023. "A Concise Review on Cathode Materials for Na-Ion Batteries." *Materials Today: Proceedings*, April. https://doi.org/10.1016/j.matpr.2023.03.401.

Shao, Gaofeng, Dorian A. H. Hanaor, Jun Wang, Delf Kober, Shuang Li, Xifan Wang, Xiaodong Shen, Maged F. Bekheet, and Aleksander Gurlo. 2020. "Polymer-Derived

SiOC Integrated with a Graphene Aerogel As a Highly Stable Li-Ion Battery Anode." *ACS Applied Materials & Interfaces* 12 (41): 46045–56. https://doi.org/10.1021/acsami.0c12376.

Share, Keith, Adam P. Cohn, Rachel Carter, Bridget Rogers, and Cary L. Pint. 2016. "Role of Nitrogen-Doped Graphene for Improved High-Capacity Potassium Ion Battery Anodes." *ACS Nano* 10 (10): 9738–44. https://doi.org/10.1021/acsnano.6b05998.

Shterenberg, Ivgeni, Michael Salama, Yossi Gofer, Elena Levi, and Doron Aurbach. 2014. "The Challenge of Developing Rechargeable Magnesium Batteries." *MRS Bulletin* 39 (5): 453–60. https://doi.org/10.1557/mrs.2014.61.

Sun, Mengxuan, Kai Yang, Nengze Wang, Lei Hu, Xiaohe Ren, Zhijie Li, Chunyang Jia, and Xiaojun Yao. 2024. "Nitrogen-Doped Graphene Enables Stable Zinc Anode for Long-Term Cycling Aqueous Zn-Ion Batteries." *Applied Surface Science* 648 (March): 159008. https://doi.org/10.1016/j.apsusc.2023.159008.

Szabo, Attila, and Neil S Ostlund. 2012. *Modern Quantum Chemistry: Introduction to Advanced Electronic Structure Theory*. Courier Corporation.

Tapia, Nelly Esther Flores, Vanessa Valverde, Gabriel Moreano, Subhash Chandra, Luis Buenaño, Ahmad Ismael Saber, Hala Bahair, Parminder Singh, and Yasser Elmasry. 2024. "The Outstanding Electrochemical Performance of Porous Hexagonal Boron Nitride as a K-Ion Battery Anode." *Inorganic Chemistry Communications* 159 (January): 111816. https://doi.org/10.1016/j.inoche.2023.111816.

Tarascon, J.-M., and M. Armand. 2001. "Issues and Challenges Facing Rechargeable Lithium Batteries." *Nature* 414 (6861): 359–67. https://doi.org/10.1038/35104644.

Thakur, Amrit Kumar, Mohammad Shamsuddin Ahmed, Jimin Park, Rajendran Prabakaran, Shaji Sidney, Ravishankar Sathyamurthy, Sung Chul Kim, Somasundaram Periasamy, Jaekook Kim, and Jang-Yeon Hwang. 2022. "A Review on Carbon Nanomaterials for <scp>K-ion</Scp> Battery Anode: Progress and Perspectives." *International Journal of Energy Research* 46 (4): 4033–70. https://doi.org/10.1002/er.7508.

Tsuji, Yuta, Yasuhiro Kitamura, Masao Someya, Toshihiko Takano, Michio Yaginuma, Kohei Nakanishi, and Kazunari Yoshizawa. 2019. "Adhesion of Epoxy Resin with Hexagonal Boron Nitride and Graphite." *ACS Omega* 4 (3): 4491–4504. https://doi.org/10.1021/acsomega.9b00129.

Tutusaus, Oscar, Rana Mohtadi, Timothy S. Arthur, Fuminori Mizuno, Emily G. Nelson, and Yulia V. Sevryugina. 2015. "An Efficient Halogen-Free Electrolyte for Use in Rechargeable Magnesium Batteries." *Angewandte Chemie International Edition* 54 (27): 7900–7904. https://doi.org/10.1002/anie.201412202.

Tyagi, Neha, and Neeraj K. Jaiswal. 2022. "Enhancing the Performance of BN Nanosheets as Promising Anode Material for Li-Ion Batteries with Carbon-Doping." *Journal of Molecular Graphics and Modelling* 115 (September): 108213. https://doi.org/10.1016/j.jmgm.2022.108213.

Wang, Haibo, Thandavarayan Maiyalagan, and Xin Wang. 2012. "Review on Recent Progress in Nitrogen-Doped Graphene: Synthesis, Characterization, and Its Potential Applications." *ACS Catalysis* 2 (5): 781–94. https://doi.org/10.1021/cs200652y.

Wang, Yusheng, Sen Wang, Nahong Song, Xiaowei Wu, Jing Xu, Shijun Luo, Bin Xu, and Fei Wang. 2024. "On Two-Dimensional Metal Borides (MBenes) as Anode Materials for Metal-Ion Batteries: A First-Principles Study." *Computational Materials Science* 233 (January): 112710. https://doi.org/10.1016/j.commatsci.2023.112710.

Watanabe, Kenji, Takashi Taniguchi, and Hisao Kanda. 2004. "Direct-Bandgap Properties and Evidence for Ultraviolet Lasing of Hexagonal Boron Nitride Single Crystal." *Nature Materials* 3 (6): 404–9. https://doi.org/10.1038/nmat1134.

Weigend, Florian, and Reinhart Ahlrichs. 2005. "Balanced Basis Sets of Split Valence, Triple Zeta Valence and Quadruple Zeta Valence Quality for H to Rn: Design and Assessment of Accuracy." *Physical Chemistry Chemical Physics* 7 (18): 3297. https://doi.org/10.1039/b508541a.

Wu, Jingxing, Yinliang Cao, Haimin Zhao, Jianfeng Mao, and Zaiping Guo. 2019. "The Critical Role of Carbon in Marrying Silicon and Graphite Anodes for High-Energy

Lithium-Ion Batteries." *Carbon Energy* 1 (1): 57–76. https://doi.org/10.1002/CEY2.2.

Wu, Jingyi, Xiongwei Li, Zhixiang Rao, Xiaoning Xu, Zexiao Cheng, Yaqi Liao, Lixia Yuan, Xiaolin Xie, Zhen Li, and Yunhui Huang. 2020. "Electrolyte with Boron Nitride Nanosheets as Leveling Agent towards Dendrite-Free Lithium Metal Anodes." *Nano Energy* 72 (June): 104725. https://doi.org/10.1016/j.nanoen.2020.104725.

Zhang, Gang, and Charles B. Musgrave. 2007. "Comparison of DFT Methods for Molecular Orbital Eigenvalue Calculations." *The Journal of Physical Chemistry A* 111 (8): 1554–61. https://doi.org/10.1021/jp061633o.